Review



# Molybdenum Disulfide as Tunable Electrochemical and Optical Biosensing Platforms for Cancer Biomarkers Detection: A Review

Ziyue Qin , Jiawei Zhang , Shuang Li *

Posted Date: 28 July 2023

doi: 10.20944/preprints202307.1977.v1

Keywords: molybdenum disulfide; electrochemical sensor; optical sensor; cancer biomarkers; detection

*Review*

# Molybdenum Disulfide as Tunable Electrochemical and Optical Biosensing Platforms for Cancer Biomarkers Detection: A Review

**Ziyue Qin [1,2], Jiawei Zhang [1,2] and Shuang Li [1,2,*]**

[1] Medical College, Tianjin University, Tianjin, 300072, China
[2] Academy of Medical Engineering and Translational Medicine, Tianjin University, Tianjin, 300072, China
* Correspondence: lishuangv@tju.edu.cn; Tel.: +86 022 83612122; Fax: +86 022 83612122

**Abstract:** Cancer is a common illness with a high mortality. Compared to traditional technologies, biomarkers detection, with low cost and simple operation, has higher sensitivity and faster speed in early screening and prognosis of cancer. Therefore, extensive research has been focused on the development of biosensors and the construction of sensing interfaces. Molybdenum disulfide ($MoS_2$) is a promising two-dimensional (2D) nanomaterial, whose unique adjustable bandgap shows excellent electronic and optical properties in the construction of biosensor interfaces. It not only has the advantages of high catalytic activity and low manufacturing costs, but also can further expand the application of hybrid structures by different functionalization, and is widely used in various biosensors fields. Herein, the application of electrochemical and optical sensing platforms based on $MoS_2$ in the detection of cancer biomarkers was comprehensively reviewed. Firstly, the structure and preparation method of $MoS_2$ were introduced, and its applicable characteristics in the field of biosensors were explored. Secondly, we comprehensively reviewed the recent construction and application of sensing platform based on $MoS_2$ in the field of cancer biomarkers detection in both electrochemical and optical aspects. The prime characteristics and application performances of $MoS_2$ and its composites were emphasized. Additionally, we also involved some other types of biosensors based on $MoS_2$. Finally, we summarized the challenges and development prospects of $MoS_2$ in the application of cancer biomarkers detection, and provided some insights for the application potential of this kind of emerging nano-materials in a broader field.

**Keywords:** molybdenum disulfide; electrochemical sensor; optical sensor; cancer biomarkers; detection

## 1. Introduction

Cancer is the world's largest cause of death and the second most common disease [1]. At present, more than 200 types of cancers have been found. In general, imaging technologies such as ultrasound, positron emission tomography (PET), magnetic resonance imaging (MRI), or computed tomography (CT) are used for early screening, and then confirmed by tissue biopsy and histology, so that patients can be treated in a timely manner, which can dramatically reduce cancer mortality [2,3]. However, traditional cancer detection methods are often invasive, expensive, complex, and time-consuming. Rapid diagnosis and early prevention are crucial for clinical treatment and management of cancer [4].Cancer biomarkers, as important components of detection, prognosis, and providing etiological analysis of cancer, are abnormal quantities of biological molecules generated by the body's response to the disease or directly by the cancer tumor itself, including DNA, RNA, genes, proteins, enzymes, peptides, exosomes, and metabolomics [5]. They typically exist in blood, urine, tears, oral fluids, and other tissues [6]. Cancer biomarker detection has accelerated the process of cancer diagnosis, and can obtain higher sensitivity and faster cancer screening. Enzyme linked immunosorbent assay (ELISA) [7], polymerase chain reaction (PCR) [8], clustered regularly interspaced short palindromic repeats Cas9 (CRISPR-Cas9) [9], loop-mediated isothermal amplification (LAMP), time-resolved

 doi:10.20944/preprints202307.1977.v1



fluorescence spectroscopy (TR-FS), radioimmunoassay (RIA) and electrophoresis [10] have been used for the detection of cancer biomarkers [11].

In recent years, compared with traditional technologies, biosensors have potential advantages such as high sensitivity and selectivity, high accuracy, low cost, fast detection, high stability, availability, and ease of operation. They play an important role in diagnosing and quantitatively analyzing biomarker concentrations, and are widely used in various fields such as healthcare, food inspection, and environmental testing [12]. Biosensors use various biomolecules as biometric recognition components, which are fixed on the sensor surface and converted into measurable electronic or optical signals through biological response with the detection target substance for cancer biomarker detection [13]. Biosensors can be divided into electrochemical, optical, mass dependent, and radiation sensitive biosensing platforms based on different transduction principles [14,15]. Developing efficient and practical biosensors usually requires consideration of the following aspects: (1) synthesis/manufacture/assembly of suitable sensing materials; (2) select appropriate recognition/capture molecules; (3) integration of sensor surfaces with biomolecules [16,17]. With the development of nanotechnology in medicine and biotechnology, more and more researchers are combining different types of nanomaterials with optical, electrical, mechanical, and magnetic sensors to design nanosensors for the detection of cancer biomarkers [18]. Nanobiosensors are generally composed of nanomaterials and a sensor based on biometric recognition elements [19]. They can be combined according to the interaction of affinity bond, covalent bond, cross-linking, capture and physical adsorption [20].

Among various nanomaterials, 2D layered nanomaterials have attracted widespread research interest due to their quantum confinement, high absorption coefficient, high specific surface area, and tunable bandgap characteristics [21]. Among them, Graphene has excellent physical properties, chemical adjustability and application potential, and its synthesis, properties and applications are widely concerned [22]. The impressive performance of Graphene in various fields has aroused a strong interest in the exploration of a wider range of 2D layered nanomaterials "beyond graphene" [23]. Transition metal dichalcogenides (TMDs), as a new class of stable inorganic graphene analogues, have been further studied. Among them, $MoS_2$ is regarded as the representative of TMDs. Its single molecular layer is composed of the atomic layer of transition metal Mo sandwiched between two sulfur elements S [24]. Mo atoms and S atoms are closely connected by forming strong covalent bond through coordination, and the interlayer is connected by weak van der Waals force. This weak connection mode between layers provides conditions for $MoS_2$ stripping to form a single-layer 2D planar structure [25], showing unique electronic, optical, mechanical and chemical properties [26–28]. Most importantly, due to the confinement of electrons/holes in ultra-thin planar structures, $MoS_2$ is highly sensitive to changes in the microenvironment [29], thus exhibiting advantages in the construction of biosensing interfaces [30,31].

A large number of literatures have reported that kinds of biosensing platforms based on $MoS_2$ are used to detect various biomarkers. Considering the needs of cancer biomarker detection in terms of high sensitivity, high reproducibility, easy processing, low cost and miniaturization. In this review, we will focus on the excellent characteristics and application performance of $MoS_2$ and its hybrid structures. We will comprehensively review and summarize the recent sensor work based on $MoS_2$ in the electrochemical and optical aspects for the detection of cancer biomarkers. Firstly, the preparation method of $MoS_2$ and the excellent applicable characteristics in the field of biosensors are explored, and the detection of cancer biomarkers by electrochemical sensing and optical sensing based on $MoS_2$ are introduced in detail respectively. Finally, we summarize the challenges and prospects of $MoS_2$ in terms of synthesis, functionalization of composite groups, and applications, and provide some insights into the enormous potential of these emerging 2D nanomaterials in the field of cancer biomarker detection.

## 2. Synthesis and characteristics of molybdenum disulfide

$MoS_2$ belongs to hexagonal lattice structure, as shown in **Figure 1**a. Its three common crystal structures are 1T, 2H and 3R, and their corresponding point groups are D6d, D6h and C3v [32]. In

Preprints (www.preprints.org) | NOT PEER-REVIEWED | Posted: 28 July 2023 doi:10.20944/preprints202307.1977.v1



addition, an additional hypothetical 2T structure of $MoS_2$ has been studied and reported [33]. Accordingly, 1, 2 and 3 represent the number of layers, T represents the triagonal configuration, H represents the hexagonal configuration, and R represents the rhombohedral configuration. The $MoS_2$ layers in the 2H, 3R, 1T, and additional 2T crystal structures are arranged in anti parallel AB, parallel ABC, parallel AA, and anti parallel AA' stacking sequences, respectively [34]. The properties of $MoS_2$ may show different characteristics according to the change of crystal structure [35]. Among these crystal structures, 2H-$MoS_2$ exhibits thermal stability and exhibits semiconductor characteristics, making it the most widely used in practical applications. While 1T-$MoS_2$ shows paramagnetism and metallicity [36], it shows metastability and is easy to convert into 2H-$MoS_2$, which facilitates the photoelectric application of $MoS_2$ [37]. In addition, the number of layers can also alter the electrical and optical properties of $MoS_2$ nanosheets. For example, reducing the thickness of $MoS_2$ nanosheets can improve conductivity and accelerate electron transfer rate [38]. The application of $MoS_2$ in electronic devices is inseparable from its electronic band structure and electronic properties dependent on the density of states. Kuc et al. calculated the electronic band structure of $MoS_2$, and obtained the electronic band structure diagram of $MoS_2$ with different thicknesses (**Figure 1**b). The indirect band gap of blocky $MoS_2$ is 1.2 eV. During the change from blocky structure to layered structure, the band gap thickness gradually increases (1.2 eV-1.9 eV) and transforms from indirect to direct band gap (1.9 eV), showing good absorption and photoluminescence characteristics [39,40]. Compared with graphene with 0 eV band gap, this adjustable band gap improves the application of $MoS_2$ materials in the field of optoelectronics [41]. The key reason for the widespread application of $MoS_2$ in optoelectronics is that it exhibits tunable band gap characteristics as it changes in size and structure. Different band gaps bring adjustable optical responsiveness, specific detection rate, and response time, thus having a wide range of applications [42].

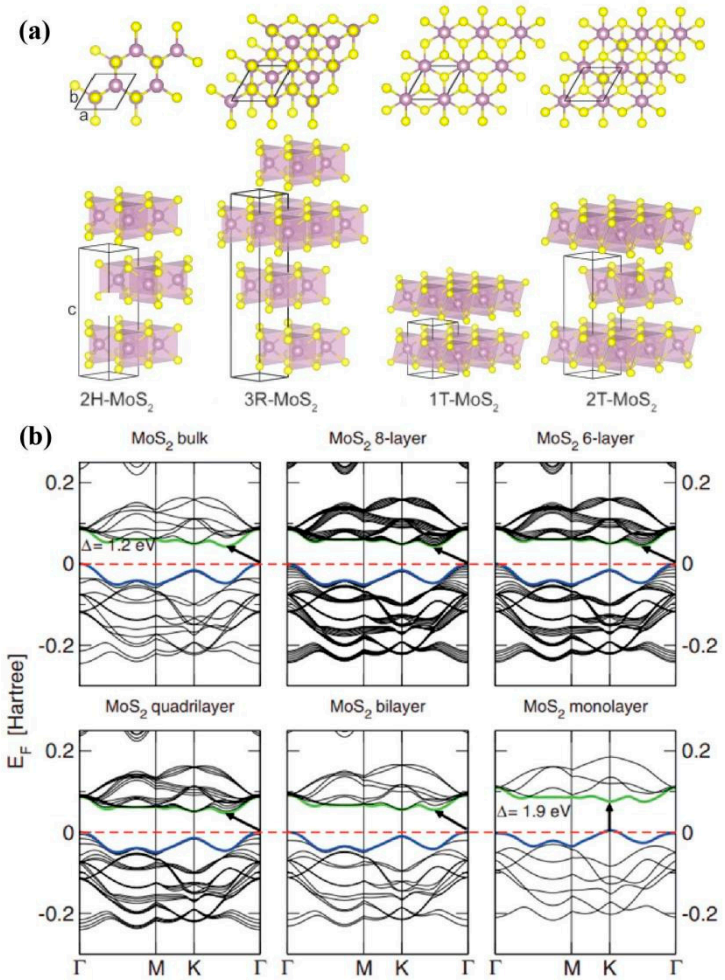

Preprints (www.preprints.org) | NOT PEER-REVIEWED | Posted: 28 July 2023 doi:10.20944/preprints202307.1977.v1



**Figure 1.** (a) Various crystal structures of $MoS_2$ (1T, 2H, 3R, 2T) [34]. Copyright 2014, Elsevier. (b) Electronic band structure diagram of $MoS_2$ with Different Thickness [40]. Copyright 2011, American Physical Society.

By controlling the synthesis conditions of $MoS_2$, various nanostructures can be synthesized. In addition to the most widely used 2D $MoS_2$ nanosheets [43], they also include structures such as 0D quantum dots (QD) [44], 1D (nanotubes) [45], and 3D (nanoflowers) [46]. Various structures exhibit different characteristics, such as the direct band gap of nanosheets, photoluminescence of quantum dots, and the high surface area and volume ratio of nanoflowers, which make $MoS_2$ exhibit unique and excellent performance in different application scenarios [47]. The synthesis methods of $MoS_2$ can be roughly divided into two categories: top-down and bottom-up (**Figure 2**). The top-down methods mainly includes mechanical exfoliation, liquid-phase exfoliation, and chemical methods. The bottom-up methods mainly includes chemical vapor deposition (CVD) and solvothermal or hydrothermal methods [48].

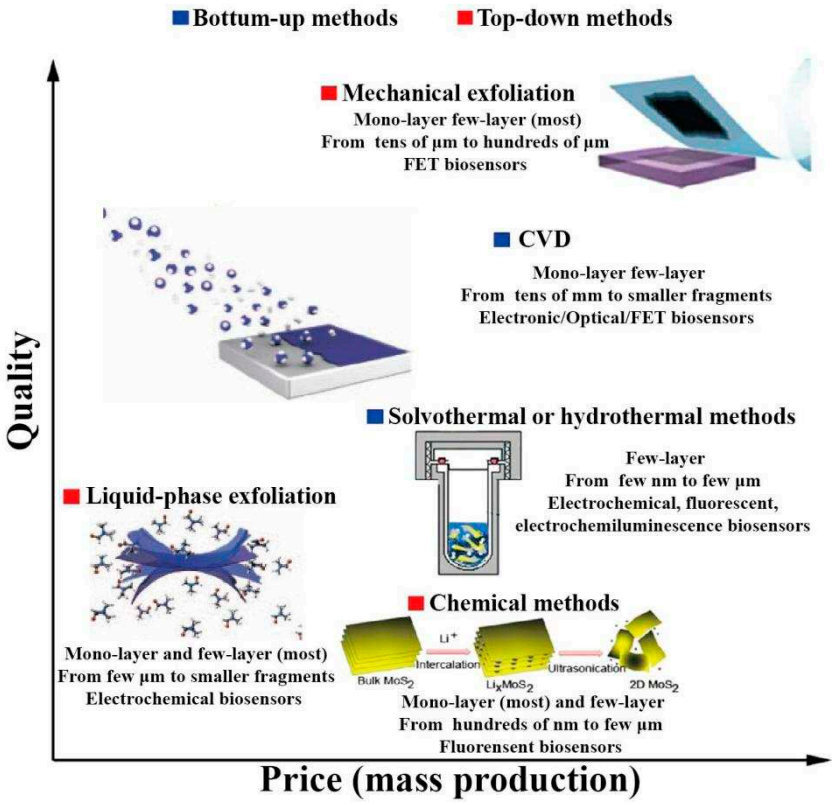


**Figure 2.** Synthesis Methods of $MoS_2$ [23,49]. Copyright 2017, Elsevier. Copyright 2012, Springer Nature.

*2.1. Top-down methods*

**Mechanical exfoliation:** As the $MoS_2$ layers are connected by the weak van der Waals force, the layered $MoS_2$ can be easily peeled off by friction of the bulk substrate $MoS_2$ with tape. The peeled tape is pressed into the appropriate substrate, and the synthetic process of $MoS_2$ mechanical exfoliation is completed by using the van der Waals force formed between $MoS_2$ and the substrate. Silicon dioxide ($SiO_2$) is currently the most widely used substrate material [50]. The mechanical exfoliation is limited by its low yield and therefore cannot be used for large-scale production. However, this method can produce layered $MoS_2$ with ideal purity and large transverse size, and is often used as a laboratory preparation method for studying the properties of $MoS_2$ materials [51].

**Liquid-phase exfoliation:** In order to overcome the low yield and difficulty in large-scale production of mechanical exfoliation, the process of stripping $MoS_2$ in solution is called liquid-phase exfoliation. Specifically, the bulk $MoS_2$ is dissolved in a suitable solution and separated from the

 doi:10.20944/preprints202307.1977.v1



layered $MoS_2$ by methods, such as bubbling, ultrasonic dispersion, grinding, and shearing [52–55]. Among them, adding surfactants [56] or bubbling bubbles [57] in the solution can help improve the stability of $MoS_2$, effectively maintain the layered structure of $MoS_2$ after peeling, and prevent it from recombining with the bulk $MoS_2$. Overall, liquid-phase exfoliation is simpler and more cost-effective than mechanical exfoliation, making it stand out in industrial applications [58].

**Chemical methods:** Chemical methods mainly rely on metal ions entering the interlayer of bulk $MoS_2$ to achieve the detachment of $MoS_2$ [58]. In the chemical stripping process, the most widely used metal ion reported is $Li^+$. However, the intercalation of $Li^+$ will simultaneously lead to the transfer of $MoS_2$ from the 2H phase exhibiting semiconductor properties to the 1T phase exhibiting metal properties, which limits the application scenarios of the generated $MoS_2$. Further research has shown that annealing at 300 °C can restore $MoS_2$ formed by $Li^+$ intercalation to the 2T phase [60]. Electrochemical methods have also emerged in the $MoS_2$ stripping process, typically using block $MoS_2$ as the cathode to achieve stripping. However, the large size and area of $MoS_2$ produced by electrochemical stripping methods are limited in their application in the biological field, thus requiring more exploration [61].

### *2.2. Bottom-up methods*

**CVD:** CVD is a typical nanomaterial growth technique that can be used to prepare high-quality $MoS_2$ with scalable size, controllable thickness, and excellent electronic properties [61]. CVD uses precursor gas molecules to adsorb on the substrate surface and generate thermal chemical decomposition reaction, thus forming high-quality layered $MoS_2$. At present, Mo precursors commonly used in CVD mainly include Mo and Molybdenum trioxide, while S precursors mainly use hydrogen sulfide gas or vaporized S [63,64]. On this basis, we further studied the CVD process of $MoS_2$ using Molybdenum(V) chloride as a precursor. The characterization results verified that this precursor can produce a larger area of high-quality single-layer $MoS_2$ films, but more precursors that can be used for CVD still need to be further explored [65]. CVD can not only produce $MoS_2$ with high film quality, but also easily functionalize $MoS_2$ by introducing other precursors during the preparation process. The entire process is very simple and convenient, and is commonly used for studying the properties of $MoS_2$ materials and constructing biosensors [66].

**Solvothermal or hydrothermal methods:** Solvothermal or hydrothermal methods are a simple, scalable, and easily controllable method for preparing $MoS_2$. The solvothermal method commonly uses solid precursors, while the hydrothermal method commonly uses liquid precursors [66]. Generally, under high temperature conditions, the molybdate that provide Mo source and the sulfides that provide S source are reacted in a polytetrafluoroethylene high-pressure reactor, and $MoS_2$ is synthesized through the generated steam pressure. In most cases, annealing treatment is required to improve its crystal quality and purity [68]. This method can effectively preserve the 2H phase of $MoS_2$ and achieve control the size parameters of $MoS_2$ to a certain degree. The harmless preparation process further preserves the biocompatibility of $MoS_2$, making it easier to obtain smaller microcrystals with high catalytic activity compared to CVD. It has great potential in constructing electrochemical and fluorescent biosensors [69].

In addition to the above methods, there are also some methods for the preparation of $MoS_2$, such as physical vapor deposition (PVD), sputtering, vapor solid growth, etc. Due to the different principles and processes of preparation methods, the generated $MoS_2$ exhibits different characteristics and is applied in different scenarios accordingly. The large size of $MoS_2$ prepared by mechanical exfoliation limits its biosensing application. Similarly, PVD exhibits harmful reverse defects compared to CVD during functionalization, which also affects its application range. Correspondingly, CVD and solution chemistry processes have been more widely promoted due to their adjustable preparation process and high-quality synthesis of $MoS_2$. The construction of electrochemical/optical sensors using the electrical/optical properties of $MoS_2$ has been extensively reported.

Preprints (www.preprints.org) | NOT PEER-REVIEWED | Posted: 28 July 2023 doi:10.20944/preprints202307.1977.v1



## 3. Electrochemical biosensors for cancer biomarkers detection based on $MoS_2$

Electrochemical sensors are mainly composed of sensitive components, signal transduction components, and nano modified electrode structures. Electrochemical analysis technology is an important detection method in the field of biomedicine. Its basic principle is to analyze the changes in current or impedance signals generated by the interaction between the analyte and the electrode surface. It can monitor the charge movement between reaction interfaces and has significant advantages in fast response [70]. In recent years, sensitive electrochemical biosensors have been developed for the detection of cancer biomarkers [71]. $MoS_2$ has been widely used in the field of electrochemical sensing of cancer biomarkers due to its excellent physical and chemical properties, excellent catalytic activity and low manufacturing costs. In this chapter, we will divide electrochemical biosensors into potentiometry, amperometry, impedimetry and photoelectrochemical (PEC) according to different signal transduction, and introduce the latest application progress of MoS2 in cancer biomarker detection.

### *3.1. Potentiometry*

Potentiometric sensors obtain information about analytes by measuring the current when potential changes, mainly including chronoamperometry (CA), cyclic voltammetry (CV), differential pulse voltammetry (DPV) and square wave voltammetry (SWV), which are widely used electrochemical analysis methods. These methods fix the biometric elements (such as antibodies, enzymes and aptamers) on the electrode surface, and monitor the current changes triggered when the analyte combines with the biometric element when the potential between the working electrode and the reference electrode remains constant. Within the linear potential range, the peak current value monitored is directly related to the concentration of the target analyte in the solution, so as to realize the detection of the target.

The electronic properties of $MoS_2$ are highly dependent on its phase structure. The ultra-thin $MoS_2$ has good performance, but it is difficult to maintain stability in an independent state and is easy to aggregate [72]. In order to improve this problem, Ying et al. [73] used liquid-phase exfoliation and surface modification to synthesize 2H-$MoS_2$ (**Figure 3**a), and used platinum nanowires (Pt NWs) arrays as nanopillars, which were added to the ultra-thin 2D $MoS_2$ interlayer to form Pt NWs arrays@$MoS_2$ nano hybrid, which improved the specific surface area and porosity, and could be used as "electronic wires" to catalyze electron transfer at the interface, avoiding folding by creating new dimensions. Thus, stability and current signal enhancement are achieved.

Two main reasons that limit the practical application of $MoS_2$ in electrochemical sensing are that the strong van der Waals force effect between layers leads to aggregation and relatively low conductivity in layers [74]. In order to overcome these shortcomings, Su et al. [75] synthesized ionic liquid (IL) functionalized AuNPs/$MoS_2$/rGO nanocomposites for sensitive detection of cancer specific target nucleolin (**Figure 3**b). The linear range of the unlabeled electrochemical sensor obtained is 0.5 nM-1.0 μM, and detection limit is 0.16 nM. Graphene has a large π electronic structure and edge, because of the synergistic effect, the combination of $MoS_2$ and graphene can significantly improve the conductivity and large surface area of $MoS_2$ [76]. In addition, the introduction of AuNPs into nanocomposites can not only fix the thioaptamer through the Au-S bond, which improves the affinity and specificity, but also enhance electron transfer and amplify the electrochemical signal.

Song et al. [77] modified rGO/$MoS_2$@polyaniline nanosheets of 3D arrays on the surface of Au electrode and further incubated carcinoembryonic antigen (CEA) specific antibodies to achieve high sensitivity detection of CEA (**Figure 3**c). First, the sensor combines rGO with $MoS_2$ to improve the stack phenomenon of $MoS_2$, thus effectively enhancing the electron transfer efficiency of the electrode. Then, polyaniline was further embedded to introduce a large number of amino groups that can bind to CEA specific antibodies, and CEA was detected using CV in a wide linear range (0.001 ng/mL-80 ng/mL), with a limit of detection (LOD) of 0.3 pg/mL. Gui et al. [78] synthesized ce-$MoS_2$/AgNR composites by using the van der Waals force and electrostatic interaction between chemically exfoliate $MoS_2$ nanosheets (ce-$MoS_2$) and Ag nanorods (AgNRs). Due to the synergistic effect, the conductivity of ce-$MoS_2$/AgNR composites have increased by nearly twice. The unlabeled

Preprints (www.preprints.org) | NOT PEER-REVIEWED | Posted: 28 July 2023 doi:10.20944/preprints202307.1977.v1



electrochemical immunosensor (EI) prepared can sensitively detect prostate specific antigen (PSA) in a wide linear range (0.1 ng/ml-1000 ng/ml) (**Figure 3**d), with a detection limit as low as 0.051 ng/ml, and have broad application potential in the clinical diagnosis of prostate cancer.

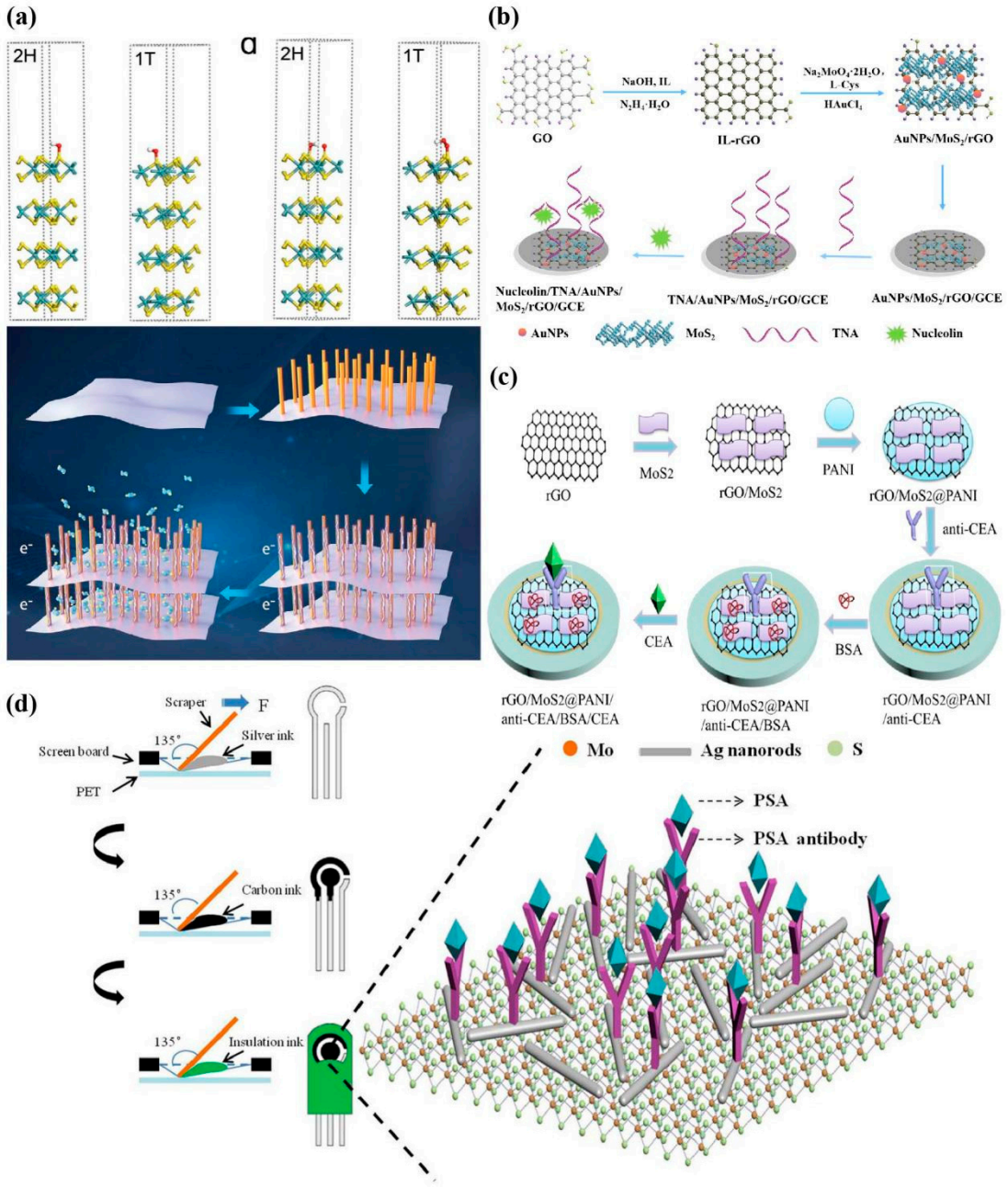


**Figure 3.** Examples of potentiometric sensors used for detecting various cancer biomarkers. (a) Optimized structure of 2H-$MoS_2$ and 1T-$MoS_2$ (upper plate) and schematic diagram of using Pt NWs arrays as nanopillars in ultra-thin $MoS_2$ films (lower plate) [73]. Copyright 2020, Wiley. (b) Schematic illustration for the synthesis of the AuNPs/MoS2/rGO nanocomposite and nucleolin electrochemical aptasensor strategy [75]. Copyright 2020, Elsevier. (c) Schematic diagram of highly sensitive detection of CEA based on rGO/$MoS_2$@polyaniline nanosheets of 3D arrays [77]. Copyright 2020, Elsevier. (d) Schematic illustration of the fabrication and PSA detection process of the EI [78]. Copyright 2020, Springer Nature.

### *3.2. Amperometry*

Amperometric sensors achieve quantitative detection of analytes by applying a constant voltage to the sensing platform to detect the current generated by the conversion of corresponding

Preprints (www.preprints.org) | NOT PEER-REVIEWED | Posted: 28 July 2023 doi:10.20944/preprints202307.1977.v1



electroactive substances. Due to their convenience and high accuracy, they are widely used in the detection of cancer biomarkers. Due to the excellent catalytic activity of $MoS_2$ for the reduction of $H_2O_2$, Ma et al. [79] used hydrothermal method to combine $MoS_2$ nanoflowers ($MoS_2$ NFs) with p-type metal semiconductor oxide cuprous oxide ($MoS_2$@$Cu_2O$) (**Figure 4**a), and at the same time, the introduction of AuNPs generated $MoS_2$@$Cu_2O$-Au complexes by Au-S bond as nanoprobes for signal amplification. The sandwich immunosensor constructed can detect the cancer marker alpha fetoprotein (AFP) of primary liver cancer in the wide linear range of 0.1 pg/mL to 50 ng/mL, demonstrating good application prospects. Ma et al. [80] have prepared a sandwich-type electrochemical immunosensor for the sensitive detection of CEA by coupling tri-metallic yolk-shell Au@AgPt nanocubes (Au@AgPt YNCs) loaded on amino-functionalized $MoS_2$ NFs ($MoS_2$ NFs/Au@AgPt YNCs) with secondary antibodies (**Figure 4**b). Due to the biphasic synergistic catalysis, the synthesized $MoS_2$ NFs/Au@AgPt YNCs as a signal label effectively catalyzes the reduction of $H_2O_2$ to amplify the current signal, and realizes the high-precision detection of CEA in the range of 10 fg/mL-100 ng/mL, with the LOD as low as 3.09 fg/mL (S/N=3). These works provide ideas for the composite modification of $MoS_2$ with different nano forms and further applications in biosensing platforms.

### *3.3. Impedimetry*

Impedance sensors are an important type of electrochemical sensing that obtains information about analytes by measuring the conductance through interface reactions on the electrode surface. This type of sensor is very sensitive to the change of electrode, and is in an advantageous position in the detection of biomarkers. Therefore, it is also widely introduced into the construction of electrochemical sensing platform for the detection of cancer biomarkers. Jia et al. [81] prepared a novel nanohybrid of polyoxometalate-derived $MoS_2$ nanosheets (pd-$MoS_2$ NSs) by a hydrothermal method, which exhibited excellent electrochemical activity and abundant catalytic sites. Furthermore, pd-$MoS_2$ NSs were vertically grown over β-FeOOH NRs (pd-$MoS_2$@β-FeOOH) serving as complementary DNA platforms for fixing oncogenes and tumor suppressor miRNA-21, using electrochemical impedance spectroscopy (EIS) to detect miRNA-21, with a LOD as low as 0.11 fM. In addition, microfluidic electrochemical immunochips have been evaluated as a powerful detection platform because of its high sensitivity, low cost, portability and easy miniaturization. Sri et al. [82] synthesized $MoS_2$ NFs by the same method, and electrophoretically deposited them on indium tin oxide (ITO) coated glass substrate. Due to the morphology of $MoS_2$ NFs, antibodies can be effectively fixed on the electrode surface through physical adsorption. The biosensor can sensitively detect tumour necrosis factor-α (TNF-α) between 1-200 pg/ml, LOD as low as 0.202 pg/ml (**Figure 4**c). Hu et al. [83] first prepared $MoS_2$ by liquid-phase exfoliation and formed a hybrid film with PDDA, designed a three-electrode system in the microfluidic chip, introduced $MoS_2$/PDDA film modified with anti-AFP as the working electrode, Ag/AgCl as the reference electrode, and ITO as the counter electrode (**Figure 4**d). The linear range of AFP detected by EIS was 0.1 ng/mL to 10 ng/mL, the LOD is 0.033 ng/mL.

### *3.4. Photoelectrochemistry (PEC)*

PEC utilizes photosensitive materials at the electrode interface as signal converters to analyze the electrical signals generated by analytes under light irradiation, combining the advantages of spectral analysis and electrochemical technology. $MoS_2$ exhibits excellent characteristics of tunable bandgap in its transition from blocky structure to layered structure. The quantum confinement effect leads to good visible light absorption and photoelectric conversion efficiency of layered $MoS_2$ as a direct bandgap semiconductor under visible light excitation, resulting in photocurrent generation. Therefore, it has been introduced into the application of photoelectrochemical sensing platforms. Hu et al. [84] utilized this mechanism to design a PEC sensing platform based on $MoS_2$/Au/GaN for high sensitivity detection of AFP (**Figure 4**e). $MoS_2$ can suppress the charge transfer of Au/GaN photoelectrodes, leading to a significant decrease in photocurrent. However, the presence of AFP can reduce the inhibitory effect on photocurrent, thereby utilizing the difference in photocurrent to detect

Preprints (www.preprints.org) | NOT PEER-REVIEWED | Posted: 28 July 2023 doi:10.20944/preprints202307.1977.v1



AFP. AFP detection is achieved in a wide linear range of 1.0-150 ng/mL, with a LOD of 0.3 ng/mL. This method has good sensitivity and high selectivity for AFP detection. Wei et al. [85] synthesized a light responsive ZnS/C/$MoS_2$ nanocomposite to construct a PEC immunosensor for detecting CEA, with a linear range of 2.0 pg/mL-10.0 ng/mL and the LOD of 1.30 pg/mL (S/N=3), showing good analytical characteristics (**Figure 4**f). In addition to the above sensing methods, other sensing methods based on $MoS_2$ are listed in the **Table 1** to detect various cancer biomarkers.

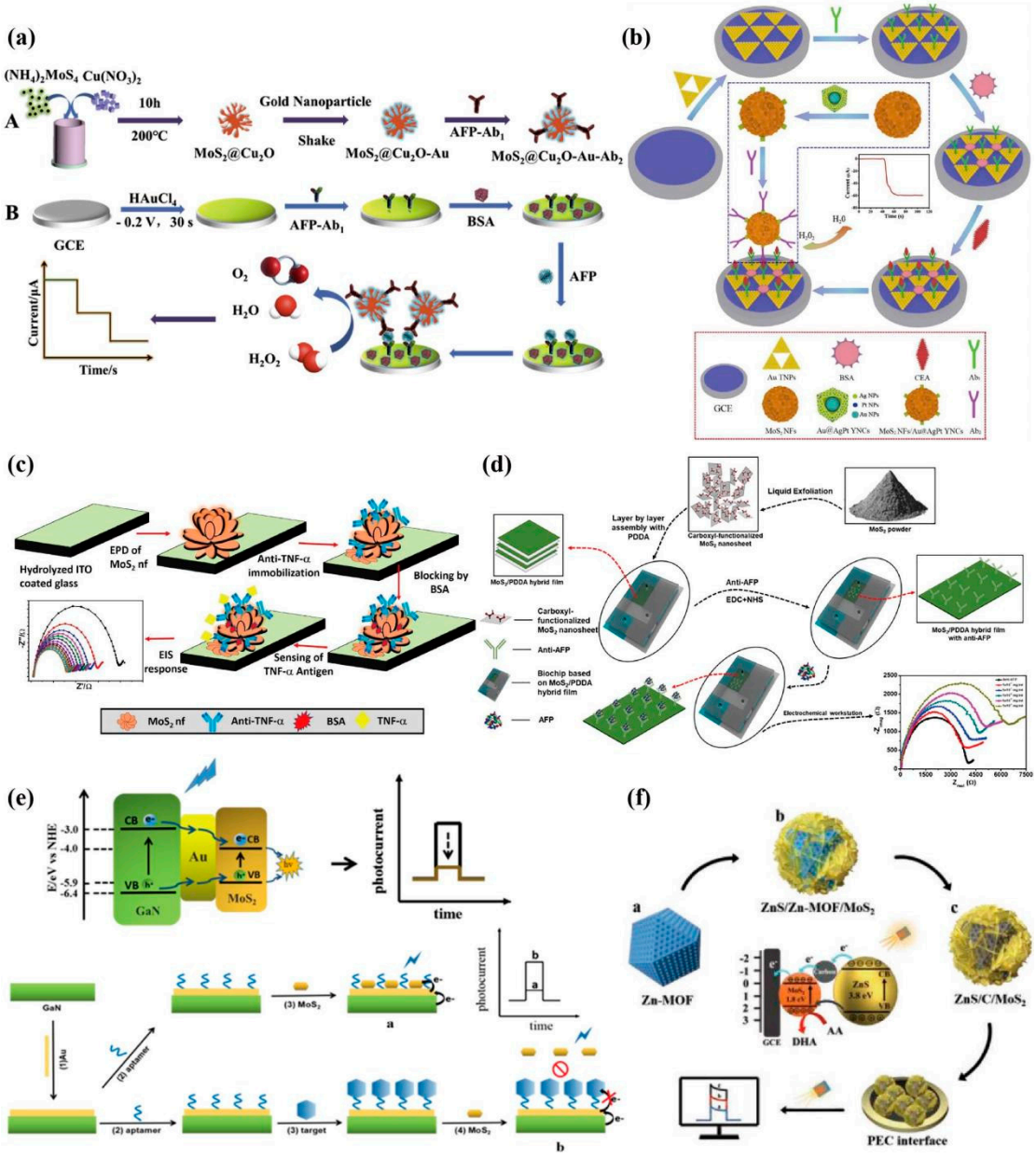


**Figure 4.** Examples of amperometric/impedance/PEC sensors used for detecting various cancer biomarkers. (a) Schematic diagram of ultrasensitive electrochemical immunosensor for AFP detection based on $MoS_2$@$Cu_2O$-Au [79]. Copyright 2019, Elsevier. (b) Schematic illustration of electrochemical immunosensor based on $MoS_2$ NFs/Au@AgPt YNCs as signal amplification label for sensitive detection of CEA [80]. Copyright 2019, Elsevier. (c) Schematic representation of BSA/anti-TNF-α/$MoS_2$ NFs/ITO immunoelectrode fabrication [82]. Copyright 2022, Elsevier. (d) Schematic illustration for self-assembly of $MoS_2$/PDDA hybrid film, microfluidic chip fabrication, anti-AFP immobilization and electrochemical detection of AFP [83]. Copyright 2020, Elsevier. (e) Charge-transfer mechanism in $MoS_2$/Au/GaN and the AFP detection schematic illustration of the PEC sensor [84]. Copyright 2021, American Chemical Society. (f) Schematic illustration of the stepwise fabrication

Preprints (www.preprints.org) | NOT PEER-REVIEWED | Posted: 28 July 2023 doi:10.20944/preprints202307.1977.v1



of ZnS/C/$MoS_2$ nanocomposite and the enhancement effect on photocurrent response [85]. Copyright 2019, Wiley.

**Table 1.** Electrochemical biosensors for cancer biomarkers detection based on $MoS_2$.

| Method | Analytes | Electrode/Label | Linear range | LOD | Ref. |
|---|---|---|---|---|---|
| Chronoamperometry | AMACR | Pt NWs array@2H-$MoS_2$/SPE | 0.70 ng/μL-12.50 ng/μL | 0.5 pg/μL | [73] |
| CV | CEA | Ab/rGO/$MoS_2$@PANI/GCE | 0.001 ng/mL-80 ng/mL | 0.3 pg/mL | [77] |
| CV | PSA | Ab/ce-$MoS_2$/AgNR/SPE | 0.1 ng/mL-1000 ng/mL | 0.051 ng/mL | [78] |
| DPV | CEA | Ab/$MoS_2$-PBNCs/GCE | 0.005 ng/mL-10 ng/mL | 0.54 pg/mL | [86] |
| DPV | CEA | Ag/$MoS_2$@$Fe_3O_4$-Ab2/CEA/Ab1/Ag/MGCE | 0.0001 ng/mL-20 ng/mL | 0.03 pg/mL | [87] |
| DPV | miRNA-182 | ssRNA/$MoS_2$/$Ti_3C_2$/GCE | 1 fM-0.1 nM | 0.43 fM | [88] |
| DPV | CEA | $MoS_2$-AuNPs/HRP-Ab2/CEA/Ab1/$MoS_2$-AuNPs/GCE | 10 fg/mL-1 ng/mL | 1.2 fg/mL | [89] |
| DPV | Nucleolin | TNA/AuNPs/$MoS_2$/rGO/GCE | 0.5 nM-1.0 μM | 0.16 nM | [75] |
| DPV | CEA | Ab/Pd@Pt/$MoS_2$-Gr/GCE | 0.00001 ng/mL-100 ng/mL | 0.005 pg/mL | [90] |
| DPV | CA125 | Ab/CuBTC@$MoS_2$-AuNPs/SPE | 0.5 mU/mL-500 U/mL | 0.5 mU/mL | [91] |
| DPV | anti-retroviral agent indinavir | ZnO NRs/$MoS_2$ NSs/SPE | 0.01-0.66 μM & 0.66-7.88 μM | 0.007 μM | [92] |
| SWV | CEA | CeO2-$MoS_2$-$Pb^{2+}$-Ab2/CEA/Ab1/AuNPs/GCE | 0.001 ng/mL-80 ng/mL | 0.3 pg/mL | [93] |
| Amperometry | CEA | Ab/Ag/$MoS_2$/rGO/GCE | 0.01 pg/mL-100 ng/mL | 1.6 fg/mL | [94] |
| Amperometry | HBeAg | Au@Pd/$MoS_2$@MWCNTs-Ab2/HBeAg/Ab1/p-GO@Au/GCE | 0.1 pg/mL-500 pg/mL | 26 fg/mL | [95] |
| Amperometry | AFP | $MoS_2$@$Cu_2O$-Au-Ab2/AFP/Ab1/AuNPs/GCE | 0.1 pg/mL-50 ng/mL | 0.037 pg/mL | [79] |
| Amperometry | AFP | Ab/Pt NDs/PDDA/$MoS_2$@PPy NTs/GCE | 50 fg/mL-50 ng/mL | 17 fg/mL | [96] |
| Amperometry | CEA | $MoS_2$ NFs/Au@AgPt YNCs -Ab2/CEA/Ab1/AuTNPs/GCE | 10 fg/mL-100 ng/mL | 3.09 fg/mL | [80] |
| EIS | CML | pDNA/PANI-$MoS_2$/ITO | $10^{-17}$ M-$10^{-6}$ M | $3\times10^{-18}$ M | [97] |
| EIS | AFP | Ab/$MoS_2$/PDDA/Ag/AgCl wire | 0.1 ng/mL-10 ng/mL | 0.033 ng/mL | [83] |
| EIS | miRNA-21 | cDNA/pd-$MoS_2$@β-FeOOH/Au | 1 fM-5 nM | 0.11 fM | [81] |
| EIS | TNF-α | $MoS_2$ NFs | 0.01-200 pg/ml | 0.202 pg/ml | [82] |
| PEC | CEA | ALP-Au-Ab2/CEA /Ab1/ZnS/C/$MoS_2$/GCE | 2.0 pg/mL-10.0 ng/mL | 1.30 pg/mL | [85] |
| PEC | SCCA | Ab/AuNPs/C/$MoS_2$/GCE | 0.005 ng/mL-8 ng/mL | 1.8 pg/mL | [98] |
| PEC | AFP | DNA/Au/GaN | 1.0 ng/mL-150 ng/mL | 0.3 ng/mL | [84] |
| PEC | MCF-7 cells | PM6:Y6/anti-EpCAM-MNs /Au NPs/Au-aptamer | 10-10000 cell/mL | 9 cell/mL | [99] |

## 4. Optical biosensors for cancer biomarkers detection based on $MoS_2$

Optical biosensors bring additional advantages in the fields of biotechnology, environmental research, disease diagnosis, and medical applications due to their high selectivity, fast, and sensitive measurement. The working principle and key performance indicators of optical biosensors largely depend on the optical transducers tightly integrated with biological sensing components [100]. Based on different biosensor elements, optical biosensors are divided into colorimetry, electrochemiluminescence (ECL), fluorescence, surface enhanced raman scattering (SERS), surface plasmon resonance (SPR) and other sensing methods. In combination with $MoS_2$, the latest application progress in cancer biomarker detection is introduced respectively.

Preprints (www.preprints.org) | NOT PEER-REVIEWED | Posted: 28 July 2023 doi:10.20944/preprints202307.1977.v1



*4.1. Colorimetry*

$MoS_2$, with its large surface area and exposed reaction sites, can be used as a nano enzyme to show the catalytic activity and excellent stability of peroxidase, and simulates natural enzymes to make the substrate color change. This feature is used to build a colorimetric sensor to detect cancer biomarkers [101,102]. Zhao et al. [103] introduced an aptamer to enhance the catalytic activity of $MoS_2$ NSs on peroxidase substrates and designed a colorimetric sensor for intuitive detection of CEA, achieving sensitivity detection of CEA by recording absorbance successfully (**Figure 5**a). The sensor exhibits a linear response in the range of 50 to 1000 ng/mL, with a LOD of 50 ng/mL, demonstrating good specificity and practical application capabilities. Shao et al. [104] utilized the high catalytic activity of $MoS_2$-AuNPs nanohybrids to reduce $NaBH_4$ to 4-NP and make the yellow solution colorless, and constructed a colorimetric immunosensor for CEA detection (**Figure 5**b). The absorbance peak intensity of the colorimetric sensor maintains a good linear relationship in the range of 5 pg/mL to 10 ng/mL, with a LOD as low as 0.5 pg/mL. Wang et al. [105] developed a new colorimetric nano biological platform for the efficient and highly sensitive capture of circulating tumor cells (CTC), in which the $MoS_2$ NSs surface is modified with two kinds of aptamer functionalized PH sensitive heterochromatic dyes used as a visual detection chip, which has good PH sensitivity and high dyeing ability.

*4.2. ECL*

ECL is a special form of chemiluminescence caused by the redox between electrogenerated high-energy radicals [106]. It does not rely on external light excitation and avoids the adverse effects of self-luminous and light scattering [107]. Therefore, it has the characteristics of precise response, easy control, low noise background signal, high sensitivity, good repeatability, and wide linear range, and has become a powerful tool for biomarkers detection and clinical diagnosis in recent years [108,109]. $MoS_2$ can effectively improve the rate of electron transfer, and is emerging in the construction of ECL sensing platform for cancer biomarkers [110]. Zhang et al. [111] used ordered mesoporous carbon-$MoS_2$ (OMC-$MoS_2$) as a sensing platform and $Cu_2O$@OMC-Ru $(bpy)_3^{2+}$ as signal tags to develop a sandwich ECL immunosensor for the detection of AFP (**Figure 5**c). As we know, $MoS_2$ NSs are easy to agglomerate, resulting in loss of activity, and the synergistic effect of nanocomposites can offset this loss of activity. OMC exhibits excellent electrocatalytic performance due to its ordered pore structure, high specific surface area, and high porosity [112]. Therefore, OMC-$MoS_2$ can synergistically increase the effective surface area and conductivity to improve sensor sensitivity. The ECL detection range of AFP is 0.1 pg/mL-10 ng/mL, with a LOD of 0.011 pg/mL (S/N=3). Liu et al. [113] synthesized $MoS_2$ NSs by the hydrothermal method, enhanced the electrochemiluminescence signal of sulfur doped boron nitrogen quantum dots (QDs) by using its strong surface plasmon coupling (SPC) light absorption effect in visible and near-infrared regions, and constructed an ECL sensing platform amplified by hybrid Chain reaction (HCR) for hepatitis C virus (HCV) genetic testing (**Figure 5**d).

Preprints (www.preprints.org) | NOT PEER-REVIEWED | Posted: 28 July 2023 doi:10.20944/preprints202307.1977.v1



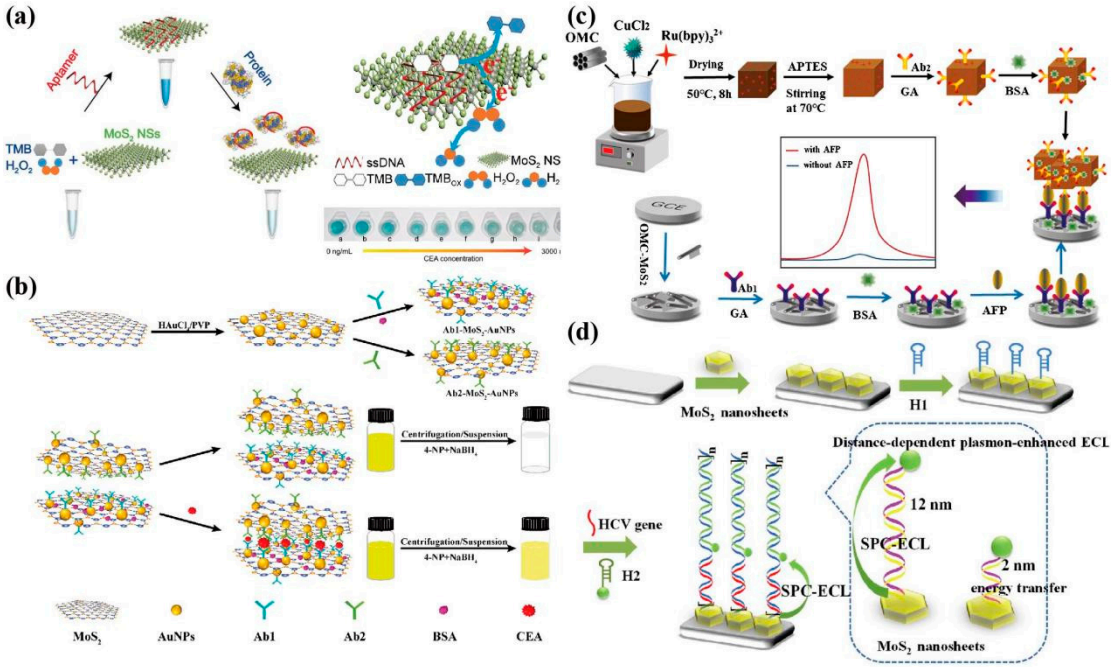


**Figure 5.** Examples of colorimetric/ECL sensors used for detecting various cancer biomarkers. (a) Schematic illustration of the colorimetric biosensor based on aptamer-modified $MoS_2$ NSs for CEA protein detection [103]. Copyright 2020, RSC Pub. (b) Preparation of $MoS_2$-AuNPs nanohybrids and Ab-$MoS_2$-AuNPs nanoprobes, and schematic illustration of the colorimetric sensor for CEA detection [104]. Copyright 2019, American Chemical Society. (c) Schematic illustration of the sandwich-configuration ECL immunoassay based on $Cu_2O$@OMC-Ru $(bpy)_3^{2+}$ and OMC-$MoS_2$ for determination of AFP [111]. Copyright 2020, Springer Nature. (d) The HCR-based sensing process and distance-dependent plasmon-enhanced ECL for HCV detection [113]. Copyright 2020, Elsevier.

*4.3. Fluorescence*

Fluorescence analysis is an advanced analytical method with high sensitivity, selectivity, and practicality, which can qualitatively and quantitatively analyze the changes in fluorescence intensity, emission spectrum, and fluorescence molecular lifetime of substances [114]. Due to the strong adsorption capacity and wide absorption spectrum of $MoS_2$ NSs to ssDNA, $MoS_2$ NSs can quench fluorescent groups with different emission wavelengths, showing unique advantages in the construction of fluorescent biosensor platforms [115]. Liang et al. [116] built a fluorescence sensing platform for the hepatocellular carcinoma (HCC) biomarker GP73 based on the Förster resonance energy transfer (FRET). Among them, utilizing synergistic effect of the $MoS_2$@rGO composites as a fluorescence receptor further enhanced the quenching effect, and the nitrogen doped graphene QDs modified by GP73 aptamer were used as fluorescence donors. The detection range was 5 ng/mL to 100 ng/mL, and the LOD was 4.54 ng/mL (S/N=3). It also showed good detection effect in human serum. Wang et al. [117] designed QD molecular beacons (QD-MBs) functionalized $MoS_2$ fluorescent probe (QD-MB@$MoS_2$) for dual detection of two kinds of miRNAs related to multiple myeloma (MM), with the LOD as low as fM level, realizing ultra-high sensitivity detection (**Figure 6**a). In addition, when the $MoS_2$ crystal becomes very thin, the transition from the indirect bandgap to the direct bandgap will produce strong fluorescence [118]. $MoS_2$ QDs have strong quantum confinement and edge effects and other photoelectric properties, and are widely used in fluorescence sensing, catalysis, biological imaging and other fields [119]. Ge et al. based on the quenching of $MoS_2$ QDs by the inner filter effect (IFE) and rolling circle amplification (RCA) technology, constructed a label-free and highly sensitive miRNA fluorescence detection platform with high selectivity and satisfactory recovery [119].

Preprints (www.preprints.org) | NOT PEER-REVIEWED | Posted: 28 July 2023 doi:10.20944/preprints202307.1977.v1



*4.4. SERS*

SERS technology can provide molecular fingerprint information, has high sensitivity and specificity, and does not cause damage to the sample, which is considered as a promising analytical technology in the field of disease analysis [120]. The SERS sensor composition mainly include substrates, target detection substances, and SERS capture probes. $MoS_2$ has been applied in the preparation of SERS capture probes due to its large specific surface area, stability, and excellent catalytic performance. Engine et al. [121] developed a SERS sandwich immunosensor for ultra sensitive detection of AFP (**Figure 6**b). Among them, $MoS_2$ is modified by monoclonal antibody as the capture probe of AFP, and its high surface area and adsorption capacity for biomolecules make the sensing interface more stable. The SERS immunosensor based on Au@AgNCs/$MoS_2$ nanocomposites has a good linear response in the range of 1 pg/ml to 10 ng/mL, with a LOD as low as 0.03 pg/mL. Pan et al. [122] developed a sensitive and direct SERS aptasensor for detecting gastric cancer exosomes. AuNSs-decorated $MoS_2$ NSs ($MoS_2$-AuNSs) surface were assembled with ROX-labeled aptamers (ROX-Apt) used as nano probes to achieve ultra sensitive capture of exosomes (**Figure 6**c). This sensor quantitatively detects gastric cancer exosomes over a wide range of SERS signals (55-5.5×$10^5$ particles/μL), with a LOD as low as 17 particles/μL, which provides a prospective platform for the early diagnosis of gastric cancer. In addition, Hilal et al. [123] developed a sandwich-type SERS immunosensor for sensitive detection of CEA, which has good selectivity and stability and is well applied in clinic.

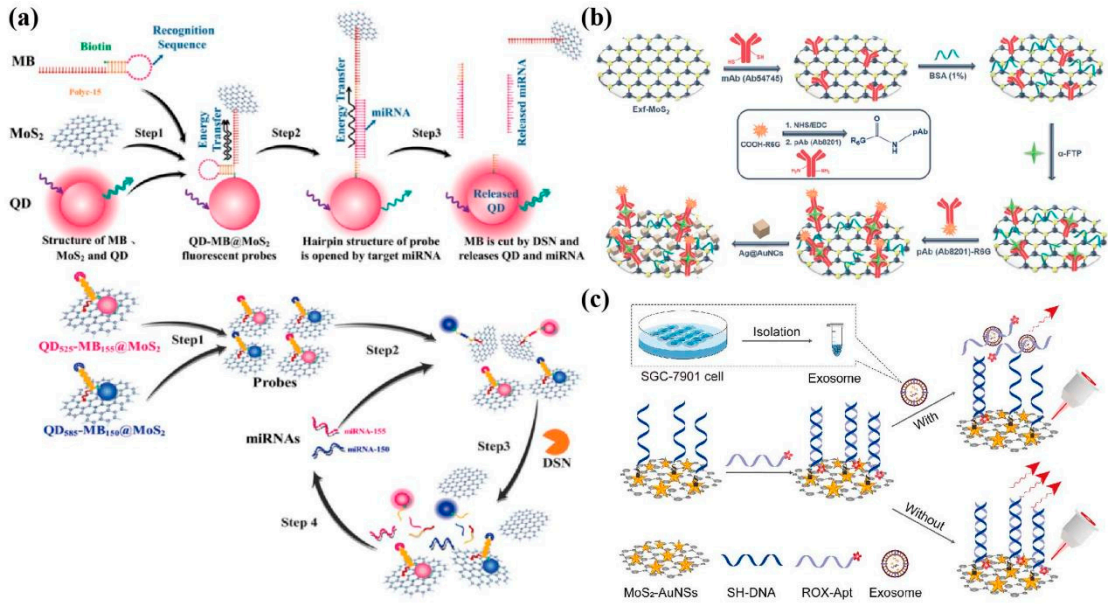


**Figure 6.** Examples of fluorescence/SERS sensors used for detecting various cancer biomarkers. (a) Schematic illustration of dual miRNAs detection by QD-MB@$MoS_2$ fluorescent probes [117]. Copyright 2022, Elsevier. (b) Schematic illustration of the SERS immunosensor based on Au@AgNCs/$MoS_2$ nanocomposites [121]. Copyright 2021, American Chemical Society. (c) Fabrication of $MoS_2$-based aptasensor for exosomes detection [122]. Copyright 2022, Elsevier.

*4.5. SPR*

SPR provides a non-invasive and label-free method to detect analytes. $MoS_2$ has a large absorption coefficient and high refractive index at 500nm, whose structure is conducive to the propagation of surface plasma. Such photoelectric characteristics enhance the SPR signals and improve the sensitivity of the sensor [124]. Therefore, the modification of $MoS_2$ is also applied in SPR sensors for cancer biomarkers detection. Chiu et al. [125] prepared $MoS_2$ by the liquid-phase exfoliation and covalently functionalize it to form carboxyl-functionalized $MoS_2$ (carboxyl-$MoS_2$) acting as a signal amplification sensing modification layer. The carboxylation modification effectively improved the sensitivity of the SPR sensor. The SPR chip based on carboxyl-$MoS_2$ is used to

Preprints (www.preprints.org) | NOT PEER-REVIEWED | Posted: 28 July 2023 doi:10.20944/preprints202307.1977.v1



specifically detect the lung cancer-associated biomarker cytokeratin 19 fragment (CYFRA21-1),which shows a wide linear range (0.05 pg/mL-100 ng/mL) and low LOD (0.05 pg/mL), and has good specificity, selectivity, sensitivity and affinity. Compared with traditional SPR bare gold chips, the SPR chip have many characteristics, such as unique glycan matrix structure, high surface area carboxylic acid groups, and excellent biological affinity. In addition to the above sensing methods, other sensing methods based on $MoS_2$ are listed in the **Table 2** to detect various cancer biomarkers.

**Table 2.** Optical biosensors for cancer biomarkers detection based on $MoS_2$.

| Method | Analytes | Electrode/Label | Linear range | LOD | Ref. |
|---|---|---|---|---|---|
| Colorimetry | CEA | Au NPs-$MoS_2$-Ab2/ CEA/Ab1/$MoS_2$-Au NPs | 5 pg/mL-10 ng/mL | 0.5 pg/mL | [104] |
| Colorimetry | CEA | DNA/$MoS_2$ NSs | 50 ng/mL-1000 ng/mL | 50 ng/mL | [103] |
| Colorimetry | CTC | TP/$SYL_3C$-$MoS_2$ | 5-$10^4$cells/mL | 2 cells/mL | [105] |
| ECL | CEA | Ab/MOF-545-Zn@MQDs/GCE | 0.18 ng/mL-1000 ng/mL | 0.45 pg/mL | [126] |
| ECL | PSA | GOD-$SiO_2$-Ab2/PSA /Ab1/$MoS_2$-AuNPs/GCE | 0.5 pg/mL-10.0 ng/mL | 0.20 pg/mL | [127] |
| ECL | HCV gene | S-BN QDs-hairpin DNA2 (H2)/$MoS_2$ Ns | 0.5 pmoL/L-1 nmoL/L | 0.17 pmoL/L. | [114] |
| ECL | HPV 16 DNA | Zn-doped $MoS_2$ QDs & QD-DNA/reductive Cu(I) particles | 0.1 nmolL-200 nmolL | 0.03 nmol/L | [128] |
| ECL | miRNA-210 | S dots/Au NP@$MoS_2$ NSs | 0.1 pM-10 nM | 0.03 pM | [129] |
| ECL | miRNA-21 | luminophore/$MoS_2$ QDs@Zeolitic Imidazolate 2 Framework-8 | Buffer (0.1 mM PBS), co-reactant (2 mM $H_2O$ ) | 14.6 aM | [130] |
| Fluorescence | CA15-3 | DNA/$MoS_2$ NSs | 0.01 U/mL-0.1 U/mL | 0.0039 U/mL | [131] |
| Fluorescence | PD-1 | $MoS_2$-NFP | 125-8000 pg/mL | 85.5 pg/mL | [132] |
| Fluorescence | miRNA-155 & miRNA-150 | QD-MB @$MoS_2$ | 10 fM-1 nM | 7.19 fM & 5.84 fM | [118] |
| SERS | CEA | $MoS_2$ NFs@Au NPs/MBA-Ab2/CEA /Ab1/$Fe_3O_4$ NPs@Au NPs/ d-$Ti_3C_2TX$ Mxene | 0.0001 ng/mL-100.0 ng/mL | 0.033 pg/mL | [125] |
| SERS | CA19-9 | R6G-tagged $MoS_2$ NF | $5\times10^{-3}$-100 IU/mL | $3.43\times10^{-4}$ IU/mL | [133] |
| SERS | exosomes | $MoS_2$-AuNSs/ROX-Apt | 55-$5.5\times10^5$ particles/μL | 17 particles/μL | [124] |
| SPR | CYFRA21-1 | Ab/COOH-$MoS_2$/Au/Cr/BK7 | 0.05 pg/mL-100 ng/mL | 0.05 pg/mL | [125] |

## 5. Miscellaneous biosensors for cancer biomarkers detection based on $MoS_2$

In addition to the two main types of cancer biomarker sensing platforms based on optics and electrochemistry, this section covers some other types of cancer biomarker sensors based on $MoS_2$. $MoS_2$ has the characteristics of direct bandgap, excellent switching ratio and high carrier mobility [134], which makes the $MoS_2$ field effect transistor (FET) biosensor have the advantages of high sensitivity, label-free biological detection, system integration and easy manufacturing. Recently, Shi et al. [135] used 2D carbon-coated $MoS_2$ NRs to form overlapping hybrid structure ($MoS_2$@C), combining with HCR, 3D DNA walker and DNA hexahedron nano framework, which established a novel fourfold amplification and self-powered intelligent sensing platform for the ultra sensitive colorimetric/electrochemical dual-mode detection of tumor suppressor miRNAs in HCC (**Figure 7**a). As a hollow network structure, $MoS_2$@C can extend the interlayer distance, not only improving the stability of the materials, but also providing more enzymes and probes binding sites. This sensor quantifies concentration of miRNAs by measuring the open circuit voltage and color changes of MBs, making it an efficient, sensitive, and highly specific sensing method. Wang et al. [136] mixed metal and semiconductor to make $MoS_2$ composite (1T-$MoS_2$) as an excellent substrate with high conductivity and electronic density of state, and combined it with the 2D graphitic carbon nitride (g-$C_3N_4$) to build a recyclable immunoassay platform for CA125 (**Figure 7**b), with the LOD as low as $4.96\times10^{-4}$ IU/mL. Basing on the excellent electronic properties and high specific recognition ability of

Preprints (www.preprints.org) | NOT PEER-REVIEWED | Posted: 28 July 2023 doi:10.20944/preprints202307.1977.v1



$MoS_2$ NSs, Yang et al. [137] constructed a FET sensor array to detect the bladder cancer biomarkers nuclear matrix protein 22 (NMP22) and cytokeratin 8 (CK8), and achieved ultra sensitive detection in a wide linear range ($10^{-6}$-$10^{-1}$ pg/mL), with LOD as low as 0.027 aM and 0.019 aM (**Figure 7**c). Zhang et al. [138] functionalized $MoS_2$ FET by coupling DNA tetrahedron and biotin-streptavidin, and detected PSA in the range of 1 fg/mL-100 ng/mL, and has broad development prospects in the field of real-time detection (**Figure 7**d). In addition to the above sensing methods, other sensing methods based on $MoS_2$ are listed in the **Table 3** to detect various cancer biomarkers.

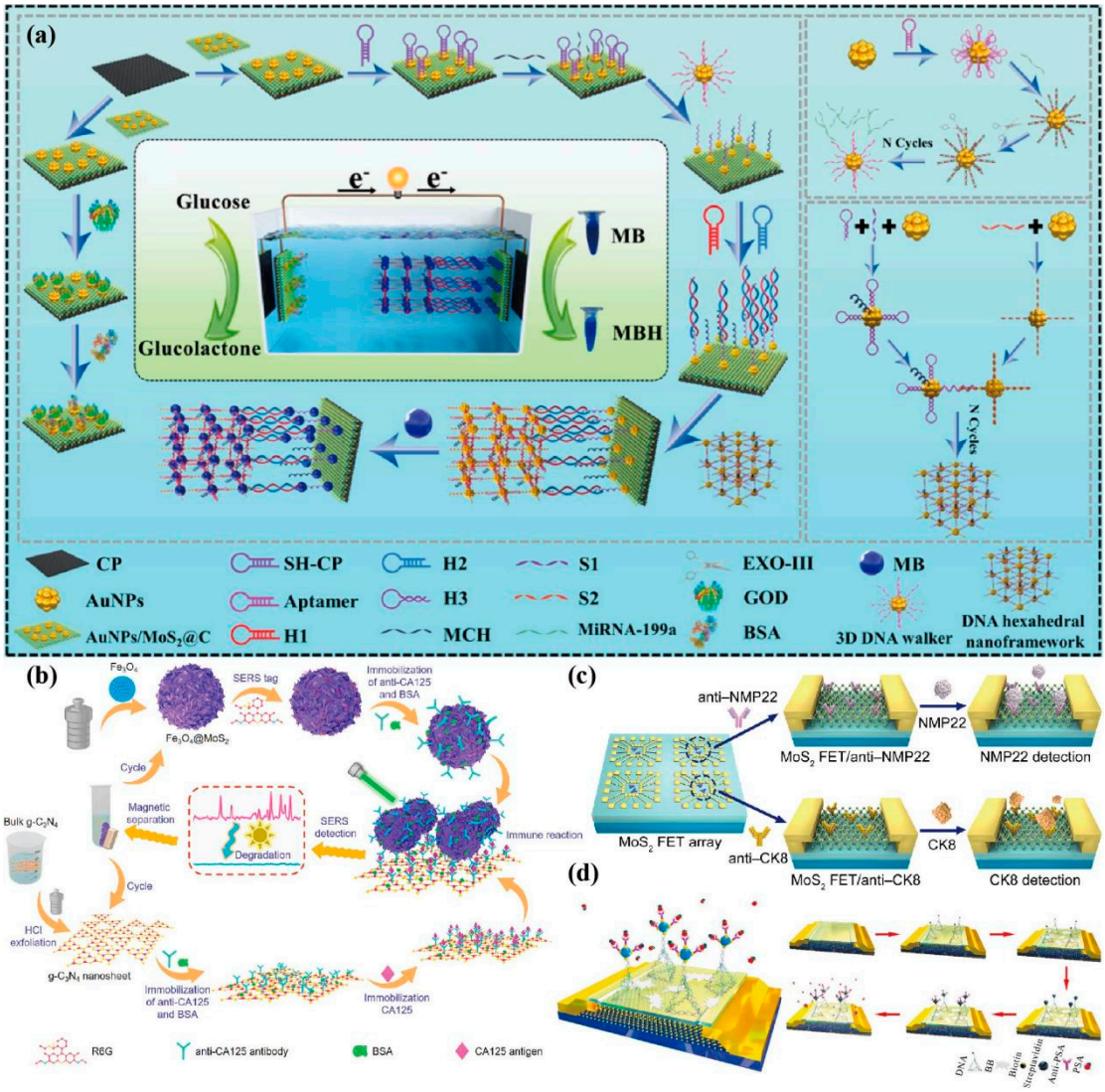


**Figure 7.** (a) Creation of ultrasensitive dual-mode approach based on self-powered sensor detecting liver cancer makers [135]. Copyright 2023, Elsevier. (b) Fabrication of $Fe_3O_4$@$MoS_2$ composites and g-C3N4 NSs as well as the protocol of recyclable SERS-based sandwich immunoassay [136]. Copyright 2023, Elsevier. (c) Schematic illustration of $MoS_2$ NSs-based FET sensor array for simultaneous detection of NMP22 and CK8 [137]. Copyright 2020, Springer Nature. (d) Surface functionalization and electrical characterization of the $MoS_2$ FET device. Schematic diagram showing the 3D structure of the functionalized $MoS_2$ biosensor (left plate). Flow chart of the device functionalization process (right plate) [138]. Copyright 2021, Elsevier.

Preprints (www.preprints.org) | NOT PEER-REVIEWED | Posted: 28 July 2023 doi:10.20944/preprints202307.1977.v1



**Table 3.** Miscellaneous biosensors for cancer biomarkers detection based on $MoS_2$.

| Method | Analytes | Electrode/Label | Linear range | LOD | Ref. |
|---|---|---|---|---|---|
| FET array | NMP22 & CK8 | $MoS_2$ NSs-FET | $10^{-6}$-$10^{-1}$ pg/mL | 0.027-0.019 aM | [137] |
| DeMEA/ microfluidic | exosome | GASI microfluidic channel/anti-EpCAM | $1\times10^{2}$-$1\times10^{9}$ exosomes/μL | 17 exosomes/μL | [139] |
| EIS/CV | $T_3$ | Au-$MoS_2$/anti-$T_3$ electrodes | 0.01-100 ng/mL | 2.5 pg/mL | [140] |
| SAW | CEA | AuNP–$MoS_2$-rGO/PI | 0.1 ng/ml-80 ng/ml. | 0.084 ng/ml | [141] |
| bio-FET | PSA | $MoS_2$/B-SA system with DNA tetrahedron | 1 fg/mL-100 ng/mL (PBS) 1 fg/mL-100 ng/mL (serum) | 1 fg/mL | [138] |
| Paper-Based/DPV | miRNA-155 miRNA-21 | AuNPs/RGO/PE AuNPs/$MoS_2$/PE | 33.8 nM-135.3 nM 135.6 nM-406.8 nM | 12.0 nM 25.7 nM | [142] |
| Microfluidic/ electrochemical/visual signal amplification/ 3D DNA walker | miRNA-141 microRNA-199a | $Bi_2S_3$@$MoS_2$ NFs/$CeO_2$ AuNPs/$MoS_2$@C | 10 fM-1 nM 0.5 fM-1 nM 0.0001-100 pM | 0.12 fM 2.65 fM 4.94 amol/L | [143] [135] |
| SERS/ELISA | ferritin | $MoS_2$ @$Fe_3O_4$/BP | 10-$10^{-4}$ μg/mL | $7.3\times10^{-5}$ μg/mL | [144] |
| SERS/ELISA | CA125 | $Fe_3O_4$@$MoS_2$/g-$C_3N_4$ NSs | $10^{-3}$-$10^{2}$ IU/mL | $4.96\times10^{-4}$ IU/mL | [136] |

## 6. Discussion and Outlook

As the representative of TMDs, unique bandgap adjustable layered structure of $MoS_2$ has shown excellent optical, electronic and mechanical properties in the construction of sensing interfaces, and has further expanded the application of $MoS_2$ as a sensing electrode in different functionalization processes. It is a promising nanomaterial to replace GO and other semiconductor devices. According to the above, the composite-based sensing interfaces built on $MoS_2$ have been widely used in the detection of different cancer biomarkers. These sensing platforms have shown good sensitivity, specificity and reproducibility, comprehensively proving the great potential of $MoS_2$ in early cancer screening. However, $MoS_2$ still faces severe challenges and further development:

Since the growth process of $MoS_2$ is uncontrollable, how to reduce the influence of impurities and lattice defects and find a large-scale and high-quality synthesis method are the fundamental issues of $MoS_2$. 2D $MoS_2$ has the defect of easy aggregation, which leads to the reduction of electrochemical activity. Accurate control of the synthesis of $MoS_2$ with uniform thickness, ideal size and colloidal stability still needs further exploration. Although these shortages can be improved by modifying $MoS_2$ with molecules, nanoparticles, or single-atom sites to form composites, achieving controllable parameters such as shape, size, charge, stability, and surface chemistry during the design process remains a major challenge [145]. Therefore, advanced synthesis techniques are needed to address these issues, such as exploring surface constrained synthesis methods and exploring better exfoliative conditions using material informatics prediction methods [146]. The covalent/non-covalent functionalization of $MoS_2$ is a powerful tool to improve dispersion and stability, and effectively expand its application by adjusting physical properties or adding new attributes [147]. For example, changing the $MoS_2$ ratio of 2H and 1T crystal structures by inducing defects or introducing additional negative charges, as well as changing the $MoS_2$ bandgap through doping, embedding, and other methods [37]. By using these approaches, $MoS_2$ can be promoted to achieve low-cost, reliable, and large-scale production, which will effectively expand the construction and application capabilities of composite-based sensing interfaces based on $MoS_2$. These new developments will drive different composite-based sensing interfaces based on $MoS_2$ into a new era.

The conversion of $MoS_2$ between different dimensions makes its characteristics and applications rich, such as semiconductor, metal or superconducting materials. For example, 2H-$MoS_2$ and 3R-$MoS_2$ can be used for dry lubricating oil [148]. The nonlinear optical properties of 3R-$MoS_2$ can be used for quantum measurements and nonlinear optical quality sensing in the biomedical field. Although $MoS_2$ shows good electronic properties, compared with silicon, its electron mobility is

 doi:10.20944/preprints202307.1977.v1



lower and its bandgap is higher, which still faces many problems in the construction of $MoS_2$ FET sensors. The conductivity of $MoS_2$ NSs is affected by temperature and thickness, which increases with increasing temperature and decreases with increasing thickness until it reaches 3D structure [149]. Furthermore, $MoS_2$ also has good characteristics of electron-spin and magnetoresistance. The research shows that $MoS_2$ has half-metallic ferromagnetism when doped with Sc, and has a unified spin-polarization value, which is conducive to the development of spintronics [150]. The key factor for the wide application of $MoS_2$ in optoelectronics is that it has an adjustable bandgap that changes with size and structure. The change of the bandgap dimension leads to the change of photoluminescence characteristics. $MoS_2$ QDs have a higher bandgap than $MoS_2$ NSs, whose optical properties can be changed by adjusting the size, or the photoluminescence intensity and emission rate can be enhanced according to the light-matter interaction. $MoS_2$ can realize broadband detection from visible light to far infrared, which is of great significance for safety, biosensors and thermal imaging, but its responsivity and detection rate are poor due to poor light absorption and large dark current [151]. We also found that the quenching ability of $MoS_2$ is easily affected by water and oxygen in the medium. Additionally, although $MoS_2$ has good biocompatibility, bioabsorption, anti-cancer and antibacterial effects in catalytic and biological activity applications, it also has high toxicity [152].

In this work, the applications of electrochemical and optical sensing platforms based on $MoS_2$ in the field of early cancer diagnosis are reviewed. In fact, $MoS_2$ shines brightly in many fields with its rich and colorful excellent characteristics. As an example, $MoS_2$ is a suitable battery electrode material, can be used for hydrogen evolution reactions, has great application prospects in biomedical fields such as cancer treatment and relevant fields of the Internet of things, and even performs a certain function in emerging technological fields such as microwave and terahertz technology. Besides, the miniaturization of sensing technology is of great significance for point of care testing (POCT). Now, with the popularity of miniaturized electronic devices, wearable, portable devices, electronic skin and other emerging technologies have been developed rapidly. Nowdays, with the popularity of miniaturized electronic devices, wearable, portable devices, electronic skin and other emerging technologies have been developed rapidly. $MoS_2$, with its good mechanical properties, has become the best candidate material for flexible sensors that can be attached to the skin to achieve non-invasive detection of biomarkers in body fluids, thus minimizing skin irritation and making it easy to measure [153]. The detection of cancer biomarkers in sweat and other bodily fluids (such as saliva and urine) based on $MoS_2$ flexible sensing interfaces needs further development, which cannot be separated from the development of electronic circuits, wireless communication units, and power supply systems.

## 7. Conclusion

In this review, we addressed the application of electrochemical and optical sensing platforms based on $MoS_2$ in the field of early cancer diagnosis, explored the improvement and application of $MoS_2$ synthesis process and material properties in the construction of biosensor platforms, and focused on the excellent characteristics of $MoS_2$ and its composites in the construction of electrochemical and optical sensing platforms and their application in the field of cancer biomarkers detection. Although $MoS_2$ still faces great challenges in synthesis technology, improving dispersion and conductivity, it has proven that unique excellent characteristics of $MoS_2$ have great potential in the field of biosensors.

**Author Contributions:** Ziyue Qin: Literature research and collation, Conceptualization, Methodology, Data curation, Writing-original draft; Jiawei Zhang: Information access, Writing-revising; Shuang Li: Structural design, Writing-review & editing, Supervision.

**Funding:** This work was supported by the National Key Research and Development Program of China (Grant No. 2022YFF1202700), the National Natural Science Foundation of China (Grant No. 82001922), the HongKong Scholars Program (Grant No. XJ2021034).

## Abbreviations

AuNPs, gold nanoparticles;
rGO, reduced graphene oxide;
PDDA, poly dimethyl diallyl ammonium chloride;
Ag/AgCl, silver/silver chloride;
ITO, indium tin oxide;
AMACR, alpha-methylacyl-CoA racemase;
NaBH4, sodium borohydride;
4-NP, 4-nitrophenol;
ssDNA, single strand DNA;
AgNCs, gold nanocubes;
AuNS, gold nanostars;
CTC, circulating tumor cells;
PD-1, programmed cell death protein 1;
CYFRA21-1, cytokeratin 19 fragment (1);
$T_3$, triiodothyronine;
DSN, duplex-specific nuclease.

## References


1. Jayanthi, V.S.; Das, A.B.; Saxena, U. Recent advances in biosensor development for the detection of cancer biomarkers. *Biosensors and Bioelectronics* **2017**, 91, 15-23. https://doi.org/10.1016/j.bios.2016.12.014
2. Hasan, M.R.; Ahommed, M.S.; Daizy, M.; Bacchu, M.S.; Ali, M.R.; Al-Mamun, M.R.; Aly Saad Aly, M.; Khan, M.Z.H.; Hossain, S.I. Recent development in electrochemical biosensors for cancer biomarkers detection. *Biosensors and Bioelectronics: X* **2021**, 8, 100075. https://doi.org/10.1016/j.biosx.2021.100075.
3. Rabie, A.M.I.; Ali, A.S.M.; Al-Zeer, M.A.; Barhoum, A.; EL-Hallouty, S.; Shousha, W.G.; Berg, J.; Kurreck, J.; Khalil, A.S.G. Spontaneous Formation of 3D Breast Cancer Tissues on Electrospun Chitosan/Poly(ethylene oxide) Nanofibrous Scaffolds. *ACS Omega* **2022**, 7 (2), 2114-2126. DOI: 10.1021/acsomega.1c05646.
4. Ranjan, R.; Esimbekova, E.N.; Kratasyuk, V.A. Rapid biosensing tools for cancer biomarkers. *Biosensors and Bioelectronics* **2017**, 87, 918-930. https://doi.org/10.1016/j.bios.2016.09.061.
5. Henry, N.L.; Hayes, D.F. Cancer biomarkers. *Mol Oncol* **2012**, 6 (2), 140-146. doi: 10.1016/j.molonc.2012.01.010.
6. Sharifi, M.; Avadi, M.R.; Attar, F.; Dashtestani, F.; Ghorchian, H.; Rezayat, S.M.; Saboury, A.A; Falahati, M. Cancer diagnosis using nanomaterials based electrochemical nanobiosensors. *Biosensors and Bioelectronics* **2019**, 126, 773-784. https://doi.org/10.1016/j.bios.2018.11.026.
7. Agnolon, V.; Contato, A.; Meneghello, A.; Tagliabue, E.; Toffoli, G.; Gion, M.; Polo, F.; Fabricio, A.S.C. ELISA assay employing epitope-specific monoclonal antibodies to quantify circulating HER2 with potential application in monitoring cancer patients undergoing therapy with trastuzumab. *Sci Rep* **2020**, 10 (1), 3016. doi: 10.1038/s41598-020-59630-y.
8. Dueck, M.E.; Lin, R.; Zayac, A.; Gallagher, S.; Chao, A.K.; Jiang, L.X.; Datwani, S.S.; Hung, P.; Stieglitz, E. Precision cancer monitoring using a novel, fully integrated, microfluidic array partitioning digital PCR platform. *Sci Rep* **2019**, 9, 19606. https://doi.org/10.1038/s41598-019-55872-7.
9. Selvakumar, S.C.; Preethi, K.A.; Ross, K.; Tusubira, D.; Khan, M.W.A.; Mani, P.; Rao, T.N.; Sekar, D. CRISPR/Cas9 and next generation sequencing in the personalized treatment of Cancer. *Mol Cancer* **2022**, 24, 21 (1), 83. doi: 10.1186/s12943-022-01565-1.
10. Udo, R.; Katsumata, K.; Kuwabara, H.; Enomoto, M.; Ishizaki, T.; Sunamura, M.; Nagakawa, Y.; Soya, R.; Sugimoto, M.; Tsuchida, A. Urinary charged metabolite profiling of colorectal cancer using capillary electrophoresis-mass spectrometry. *Sci Rep* **2020**, 10 (1), 21057. doi: 10.1038/s41598-020-78038-2.
11. Barhoum, A.; Altintas, Z.; Shalini Devi, K.S.; Forster, R.J. Electrochemiluminescence biosensors for detection of cancer biomarkers in biofluids: Principles, opportunities, and challenges. *Nano Today* **2023**, 50, 101874. https://doi.org/10.1016/j.nantod.2023.101874.
12. Yang, G.J.; Xiao, Z.Q.; Tang, C.L.; Deng, Y.; Huang, H.; He, Z.Y. Recent advances in biosensor for detection of lung cancer biomarkers. *Biosensors and Bioelectronics* **2019**, 141, 111416. https://doi.org/10.1016/j.bios.2019.111416.

13. Thévenot, D.R.; Toth, K.; Durst, R.A.; Wilson, G.S. Electrochemical biosensors: recommended definitions and classification. *Biosens Bioelectron* **2001**, 16 (1-2), 121-131. doi: 10.1016/s0956-5663(01)00115-4. PMID: 11261847.
14. Choi, S.; Goryll, M.; Sin, L.Y.M.; Wong, P.K.; Chae, J. Microfluidic-based biosensors toward point-of-care detection of nucleic acids and proteins. *Microfluid Nanofluidics* **2011**, 10 (2), 231-247. doi: 10.1007/s10404-010-0638-8.
15. Kukkar, M.; Tuteja, S.K.; Sharma, A.L.; Kumar, V.; Paul, A.K.; Kim, Ki-H.; Sabherwal, P.; Deep, A. A New Electrolytic Synthesis Method for Few-Layered MoS2 Nanosheets and Their Robust Biointerfacing with Reduced Antibodies. *ACS Applied Materials & Interfaces* **2016**, 8 (26), 16555-16563. DOI: 10.1021/acsami.6b03079
16. Turner, A.P. Biosensors: sense and sensibility. *Chem Soc Rev.* **2013**, 42 (8), 3184-3196. doi: 10.1039/c3cs35528d.
17. Vaddiraju, S.; Legassey, A.; Wang, Y.; Qiang, L.; Burgess, D.J.; Jain, F. Papadimitrakopoulos F. Design and fabrication of a high-performance electrochemical glucose sensor. *J Diabetes Sci Technol* **2011**, 5 (5), 1044-1051. doi: 10.1177/193229681100500504.
18. Bozal-Palabiyik, B.; Uslu, B.; Marrazza, G. Chapter 11 - Nanosensors in Biomarker Detection. *New Developments in Nanosensors for Pharmaceutical Analysis, Academic Press* **2019**, 327-380. https://doi.org/10.1016/B978-0-12-816144-9.00011-0.
19. Kausar, M. Pesticidal activity of Pakistani Bacillus thuringiensis isolates against Helicoverpa armigera (Hubner) and Earias vittella (Lepidoptera: Noctuidae). *IOSR Journal of Pharmacy and Biological Sciences* **2013**, 4, 9-12. DOI:10.9790/3008-0460912.
20. Kaya, S.I.; Ozcelikay, G.; Mollarasouli, F.; Bakirhan, N.K.; Ozkan, S.A. Recent achievements and challenges on nanomaterial based electrochemical biosensors for the detection of colon and lung cancer biomarkers. *Sensors and Actuators B: Chemical* **2022**, 351, 130856. https://doi.org/10.1016/j.snb.2021.130856.
21. Nawz, T.; Safdar, A.; Hussain, M.; Sung Lee, D.; Siyar, M. Graphene to Advanced $MoS_2$: A Review of Structure, Synthesis, and Optoelectronic Device Application. *Crystals* **2020**, 10, 902. https://doi.org/10.3390/cryst10100902.
22. Zhu, Y.; Murali, S.; Cai, W.; Li, X.; Suk, J.W.; Potts, J.R.; Ruoff, R.S. Graphene and graphene oxide: synthesis, properties, and applications. *Adv Mater* **2010**, 22 (35), 3906-3924. doi: 10.1002/adma.201001068.
23. Gan, X.R.; Zhao, H.M.; Quan, X. Two-dimensional MoS2: A promising building block for biosensors. *Biosensors and Bioelectronics* **2017**, 89, 1, 56-71. https://doi.org/10.1016/j.bios.2016.03.042.
24. Samadi, M.; Sarikhani, N.; Zirak, M.; Zhang, H.; Zhang, H.L.; Moshfegh, A.Z. Group 6 transition metal dichalcogenide nanomaterials: synthesis, applications and future perspectives. *Nanoscale Horiz* **2018**, 3 (2), 90-204. doi: 10.1039/c7nh00137a.
25. Joswig, J.O.; Lorenz, T.; Wendumu, T.B.; Gemming, S.; Seifert, G. Optics, mechanics, and energetics of two-dimensional MoS2 nanostructures from a theoretical perspective. *Acc Chem Res* **2015**, 48 (1), 48-55. doi: 10.1021/ar500318p.
26. Ataca, C.; Şahin, H.; Ciraci, S. Stable, Single-Layer MX2 Transition-Metal Oxides and Dichalcogenides in a Honeycomb-Like Structure. *The Journal of Physical Chemistry C* **2012**, 116 (16), 8983-8999. DOI: 10.1021/jp212558p.
27. Lee, C.; Yan, H.; Brus, L.E.; Heinz, T.F.; Hone, J.; Ryu, S. Anomalous lattice vibrations of single- and few-layer MoS2. ACS Nano 2010, 4 (5), 2695-2700. doi: 10.1021/nn1003937.
28. Huang, Y.H.; Peng, C.C.; Chen, R.S.; Huang, Y.S.; Ho; C.H. Transport properties in semiconducting NbS2 nanoflakes. *Appl. Phys. Lett.* **2014**, 105 (9): 093106. https://doi.org/10.1063/1.4894857
29. Chen, F.; Xia, J.; Ferry, D.K.; Tao, N. Dielectric screening enhanced performance in graphene FET. *Nano Lett.* **2009**, 9 (7), 2571-2574. doi: 10.1021/nl900725u.
30. Kalantar-zadeh, K.; Ou, J.Z. Biosensors Based on Two-Dimensional $MoS_2$. *ACS Sensors* **2016**, 1 (1), 5-16. DOI: 10.1021/acssensors.5b00142.
31. Zhang, W.; Zhang, P.; Su, Z.; Wei, G. Synthesis and sensor applications of MoS2-based nanocomposites. *Nanoscale* **2015**, 7 (44), 18364-18378. doi: 10.1039/c5nr06121k.
32. Krishnan, U.; Kaur, M.; Singh, K.; Kumar, M.; Kumar, A. A synoptic review of MoS2: Synthesis to applications. *Superlattices and Microstructures* **2019**, 128, 274-297. https://doi.org/10.1016/j.spmi.2019.02.005.
33. Andrey, N.; Gotthard Seifert, E. Density-functional study of LixMoS2 intercalates ($0 \leqslant x \leqslant 1$). *Computational and Theoretical Chemistry* **2012**, 999, 13-20. https://doi.org/10.1016/j.comptc.2012.08.005.

34. Mortazavi, M.; Wang, C.; Deng, J.K.; Shenoy, V.B.; Medhekar, N.V. Ab initio characterization of layered MoS2 as anode for sodium-ion batteries. *Journal of Power Sources* **2014**, 268, 279-286. https://doi.org/10.1016/j.jpowsour.2014.06.049.
35. Zhao, W.; Pan, J.; Fang, Y.; Che, X.; Wang, D.; Bu, K.; Huang, F. Metastable MoS2 : Crystal Structure, Electronic Band Structure, Synthetic Approach and Intriguing Physical Properties. *Chemistry* **2018**, 24 (60), 15942-15954. doi: 10.1002/chem.201801018.
36. Shi, S.L.;Sun, Z.X.; Hu, Y.H. Synthesis, stabilization and applications of 2-dimensional 1T metallic MoS2. *Journal of Materials Chemistry A* **2018**, 6, 47. http://dx.doi.org/10.1039/C8TA08152B.
37. Sha, R.; Bhattacharyya, T.K. MoS2-based nanosensors in biomedical and environmental monitoring applications. *Electrochimica Acta* **2020**, 349, 136370. https://doi.org/10.1016/j.electacta.2020.136370.
38. Tang, H.; Morrison, S.R. Optimization of the anisotropy of composite MoS2 films. *Thin Solid Films* **1993**, 227 (1), 90-94. https://doi.org/10.1016/0040-6090(93)90190-Z.
39. Sundaram, R.S.; Engel, M.; Lombardo, A.; Krupke, R.; Ferrari, A.C.; Avouris, P.; Steiner, M. Electroluminescence in single layer MoS2. *Nano Lett.* **2013**, 13 (4), 1416-1421. doi: 10.1021/nl400516a.
40. Kuc, A.;Zibouche, N.;Heine, T. Influence of quantum confinement on the electronic structure of the transition metal sulfide. *Phys. Rev. B* **2011**, 83, 24, 245213. https://link.aps.org/doi/10.1103/PhysRevB.83.245213
41. Zhang, X.; Biekert, N.; Choi, S.; Naylor, C.H.; De-Eknamkul, C.; Huang, W.; Zhang, X.; Zheng, X.; Wang, D.; Johnson, A.T.C.; et al. Dynamic Photochemical and Optoelectronic Control of Photonic Fano Resonances via Monolayer MoS2 Trions. *Nano Lett* **2018**, 18 (2), 957-963. doi: 10.1021/acs.nanolett.7b04355.
42. Nalwa, H.S. A review of molybdenum disulfide (MoS2) based photodetectors: from ultra-broadband, self-powered to flexible devices. *RSC Adv.* **2020**, 10 (51), 30529-30602. doi: 10.1039/d0ra03183f.
43. Lee, H.P.;, Gaharwar, A.K. Light-Responsive Inorganic Biomaterials for Biomedical Applications. *Adv Sci (Weinh).* **2020**, 7 (17), 2000863. doi: 10.1002/advs.202000863.
44. Gopalakrishnan, D.; Damien, D.; Shaijumon, M.M. MoS2 quantum dot-interspersed exfoliated MoS2 nanosheets. *ACS Nano.* **2014**, 8 (5), 5297-303. doi: 10.1021/nn501479e.
45. Nath, M.; Govindaraj, A.; Rao, C. Simple Synthesis of MoS2 and $WS_2$ Nanotubes. *Advanced Materials.* **2001**, 13, 283-286. 10.1002/1521-4095(200102)13:4<283::AID-ADMA283>3.0. CO;2-H.
46. Lee, H.P.; Lokhande, G.; Singh, K.A.; Jaiswal, M.K.; Rajput, S.; Gaharwar, A.K. Light-Triggered In Situ Gelation of Hydrogels using 2D Molybdenum Disulfide (MoS2) Nanoassemblies as Crosslink Epicenter. *Adv Mater.* **2021**, 33 (23), e2101238. doi: 10.1002/adma.202101238.
47. Shounak, R.; Kaivalya, A.D.; Singh, K.A.; Lee, H.P.; Jaiswal, A.; Gaharwar, A.K. Nano-bio interactions of 2D molybdenum disulfide. *Advanced Drug Delivery Reviews* **2022**, 187, 114361. https://doi.org/10.1016/j.addr.2022.114361.
48. Najmaei, S.; Yuan, J.; Zhang, J.; Ajayan, P.; Lou, J. Synthesis and defect investigation of two-dimensional molybdenum disulfide atomic layers. *Acc Chem Res.* **2015**, 48 (1), 31-40. doi: 10.1021/ar500291j.
49. Novoselov, V, K.S.; Fal'ko, L.; Colombo, I.; Gellert, P.R.; Schwab, M.G.; Kim, K. A roadmap for graphene. *Nature* **2012**, 490, 192-200. https://doi.org/10.1038/nature11458. Copyright 2012, Springer Nature.
50. Magda, G.Z.; Pető, J.; Dobrik, G.; Hwang, C.; Biró, L.P.; Tapasztó, L. Exfoliation of large-area transition metal chalcogenide single layers. *Sci Rep.* **2015**, 5, 14714. doi: 10.1038/srep14714.
51. Matte, H.R.; Gomathi, A.; Manna, A.K.; Late, D.J.; Datta, R.; Pati, S.K.; & Rao, C.N. MoS2 and WS2 analogues of graphene. *Angewandte Chemie* **2010**, 49, 24, 4059-4062. DOI:10.1002/anie.201000009.
52. Varrla, E.; Backes, C.; Paton, K.R.; Harvey, A.; Gholamvand, Z.; McCauley, J.; Coleman, J.N. *Chemistry of Materials* **2015**, 27 (3), 1129-1139. DOI: 10.1021/cm5044864.
53. Forsberg, V.; Zhang, R.; Bäckström, J.; Dahlström, C.; Andres, B.; Norgren ,M.; Andersson, M.; Hummelgård, M.; Olin, H. Exfoliated MoS2 in Water without Additives. *PLoS One.* **2016**, 11 (4), e0154522. doi: 10.1371/journal.pone.0154522.
54. Varrla, E.; Backes, C.; Paton, K.R.; Harvey, A.; Gholamvand Z.; McCauley, J.; Coleman, J.N. Large-Scale Production of Size-Controlled MoS2 Nanosheets by Shear Exfoliation. *Chemistry of Materials* **2015**, 27 (3), 1129-1139. DOI: 10.1021/cm5044864.
55. Paton, K.R.; Varrla, E.; Backes, C.; Smith, R.J.; Khan, U.; O'Neill, A.; Boland, C.; Lotya, M.; Istrate, O.M.; King, P.; et al. Scalable production of large quantities of defect-free few-layer graphene by shear exfoliation in liquids. *Nature Mater* **2014**, 13, 624-630. https://doi.org/10.1038/nmat3944.

56. Zhang, M.; Howe, R.C.T.; Woodward, R.I.; Kelleher, E.J.R.; Torrisi, F.; Hu, G.; Popov, S.V.; Taylor, J.R.; Hasan, T. Solution processed MoS2-PVA composite for sub-bandgap mode-locking of a wideband tunable ultrafast Er:fiber laser. *Nano Res.* **2015**, 8, 1522-1534. https://doi.org/10.1007/s12274-014-0637-2.
57. Liu, N.; Kim, P.; Kim, J.H.; Ye J.H.; Kim, S.; Lee, C.J. Large-area atomically thin MoS2 nanosheets prepared using electrochemical exfoliation. *ACS Nano.* **2014**, 8 (7), 6902-6910. DOI: 10.1021/nn5016242. PMID: 24937086.
58. Coleman, J.N.; Lotya, M.; O'Neill, A.; Bergin, S.D.; King, P.J.; Khan, U.; Young, K.; Gaucher, A.; De, S.; Smith, R.J.; et al. Two-dimensional nanosheets produced by liquid exfoliation of layered materials. *Science.* **2011**, 331 (6017), 568-571. doi: 10.1126/science.1194975.
59. Eda, G.; Yamaguchi, H.; Voiry, D.; Fujita, T.; Chen, M.; Chhowalla, M. Photoluminescence from chemically exfoliated MoS2. *Nano Lett.* **2011**, 11 (12), 5111-5116. doi: 10.1021/nl201874w.
60. Fan, X.B.; Xu, P.T.; Zhou, D.; Sun, Y.F.; Li, Y.G.C.; Nguyen, M.A.T.; Terrones, M.; Mallouk, T.E. Fast and Efficient Preparation of Exfoliated 2H MoS2 Nanosheets by Sonication-Assisted Lithium Intercalation and Infrared Laser-Induced 1T to 2H Phase Reversion. *Nano Letters* **2015**, 15 (9), 5956-5960. DOI: 10.1021/acs.nanolett.5b02091.
61. Zeng, Z.; Yin, Z.; Huang, X.; Li, H.; He, Q.; Lu, G.; Boey, F.; Zhang, H. Single-Layer Semiconducting Nanosheets: High-Yield Preparation and Device Fabrication. *Angew. Chem. Int. Ed.* **2011**, 50, 11093-11097. https://doi.org/10.1002/anie.201106004.
62. Shi, Y.M.; Li, H.N.; Li, L.J. Recent advances in controlled synthesis of two-dimensional transition metal dichalcogenides via vapour deposition techniques. *Chemical Society Reviews* **2015**, 44, 9. http://dx.doi.org/10.1039/C4CS00256C.
63. Zhan, Y.; Liu, Z.; Najmaei, S.; Ajayan, P.M.; Lou, J. Large-area vapor-phase growth and characterization of MoS(2) atomic layers on a SiO(2) substrate. *Small.* **2012**, 8 (7), 966-971. doi: 10.1002/smll.201102654.
64. Lin, Y.C.; Zhang, W.J.; Huang, J.K.; Liu, K.K.; Lee, Y.H.; Liang, C.T.; Chu, C.W.; Li, L.J. Wafer-scale MoS2 thin layers prepared by MoO3 sulfurization. *Nanoscale* **2012**, 4, 20. http://dx.doi.org/10.1039/C2NR31833D.
65. Endler, I.; Leonhardt, A.; König, U.; van den Berg, H.; Pitschke, W.; Sottke, V. Chemical vapour deposition of MoS2 coatings using the precursors MoCl5 and H2S. *Surface and Coatings Technology* **1999**, 120-121, 482-488. https://doi.org/10.1016/S0257-8972(99)00413-2.
66. Liu, H.F.; Wong, S.L.; Chi, D.Z. CVD Growth of MoS2-based Two-dimensional Materials. *Chem. Vap. Deposition* **2015**, 21, 241-259. https://doi.org/10.1002/cvde.201500060.
67. Vattikuti, S.V.P.; Byon, C.; Reddy, C.V.; Venkatesh, B.; Shim J. Synthesis and structural characterization of MoS2 nanospheres and nanosheets using solvothermal method. *J Mater Sci* **2015**, 50, 5024-5038. https://doi.org/10.1007/s10853-015-9051-8.
68. Liao, H.W.; Wang, Y.F.; Zhang, S.Y.; Qian, Y.T. A Solution Low-Temperature Route to MoS2 Fiber. *Chemistry of Materials* **2001**, 6, 8, 13. doi: 10.1021/cm000602h.
69. Jeong, S.; Yoo, D.; Jang, J.; Kim, M.Y.; Cheon, J. Well-Defined Colloidal 2-D Layered Transition-Metal Chalcogenide Nanocrystals via Generalized Synthetic Protocols. *Journal of the American Chemical Society* **2012**, 134 (44), 18233-18236. DOI: 10.1021/ja3089845.
70. Zhang, Z.; Li, Q.; Du, X.; Liu, M. Application of electrochemical biosensors in tumor cell detection. *Thorac Cancer.* **2020**, 11 (4), 840-850. doi: 10.1111/1759-7714.13353.
71. Chai, H.; Tang, Y.G.; Guo, Z.Z.; Miao, P. Ratiometric Electrochemical Switch for Circulating Tumor DNA through Recycling Activation of Blocked DNAzymes. *Analytical Chemistry* **2022**, 94 (6), 2779-2784. DOI: 10.1021/acs.analchem.1c04037.
72. Zhang, S.; Wang, J.; Torad, N.L.; Xia, W.; Aslam, M.A.; Kaneti, Y.V.; Hou, Z.; Ding, Z.; Da, B.; Fatehmulla, A.; et al. Rational Design of Nanoporous MoS2/VS2 Heteroarchitecture for Ultrahigh Performance Ammonia Sensors. *Small.* **2020**, 16 (12), e1901718. doi: 10.1002/smll.201901718.
73. Ying, Z.; Feng, L.; Ji, D.72; Zhang, Y.; Chen, W.; Dai, Y.; Janyasupab, M.; Li, X.; Wen, W.; Liu, C.C. Phase-Regulated Sensing Mechanism of MoS2 Based Nanohybrids toward Point-of-Care Prostate Cancer Diagnosis. *Small.* **2020**, 16 (18), e2000307. doi: 10.1002/smll.202000307.
74. Li, F.; Zhang, L.; Li, J.; Lin, X.Q.; Li, X.Z.; Fang, Y.Y.; Huang, J.W.; Li, W.Z.; Tian, M.; Jin, J.; Li, R. Synthesis of Cu–MoS2/rGO hybrid as non-noble metal electrocatalysts for the hydrogen evolution reaction. *Journal of Power Sources* **2015**, 292, 15-22. https://doi.org/10.1016/j.jpowsour.2015.04.173.

75. Su, X.J.; Han, Y.J.; Liu, Z.G.; Fan, L.F.; Guo, Y.J. One-pot synthesized AuNPs/MoS2/rGO nanocomposite as sensitive electrochemical aptasensing platform for nucleolin detection. *Journal of Electroanalytical Chemistry* **2020**, 859, 113868. https://doi.org/10.1016/j.jelechem.2020.113868.
76. Jing, P.; Yi, H.; Xue, S.; Chai, Y.; Yuan, R.; Xu, W. A sensitive electrochemical aptasensor based on palladium nanoparticles decorated graphene-molybdenum disulfide flower-like nanocomposites and enzymatic signal amplification. *Anal Chim Acta*. **2015**, 853, 234-241. doi: 10.1016/j.aca.2014.10.003.
77. Song, Y.J.; Cao, K.H.; Li, W.J.; Ma, C.Y.; Qiao, X.W.; Li, H.L.; Hong, C.G. Optimal film thickness of rGO/MoS2 @ polyaniline nanosheets of 3D arrays for carcinoembryonic antigen high sensitivity detection. *Microchemical Journal* **2020**, 155, 104694. https://doi.org/10.1016/j.microc.2020.104694.
78. Gui, J.C.; Han, L.; Du, C.X.; Yu, X.N.; Hu, K.; Li, L.H. An efficient label-free immunosensor based on ce-MoS2/AgNR composites and screen-printed electrodes for PSA detection. *J Solid State Electrochem* **2021**, 25, 973-982. https://doi.org/10.1007/s10008-020-04872-z.
79. Ma, N.; Zhang, T.; Fan, D.W.; Kuang, X.; Ali, A.; Wu, D.; Wei, Q. Triple amplified ultrasensitive electrochemical immunosensor for alpha fetoprotein detection based on MoS2@Cu2O-Au nanoparticles. *Sensors and Actuators B: Chemical* **2019**, 297, 126821. https://doi.org/10.1016/j.snb.2019.126821.
80. Ma, E.; Wang, P.; Yang, Q.S.; Yu, H.X.; Pei, F.B.; Li, Y.Y.; Liu, Q.; Dong, Y.H. Electrochemical immunosensor based on MoS2 NFs/Au@AgPt YNCs as signal amplification label for sensitive detection of CEA. *Biosensors and Bioelectronics* **2019**, 142, 111580,https://doi.org/10.1016/j.bios.2019.111580.
81. Jia, Q.J.; Huang, S.J.; Hu, M.Y.; Song, Y.P.; Wang, M.H.; Zhang, Z.H.; He, L.H. Polyoxometalate-derived MoS2 nanosheets embedded around iron-hydroxide nanorods as the platform for sensitively determining miRNA-21. *Sensors and Actuators B: Chemical* **2020**, 323, 128647. https://doi.org/10.1016/j.snb.2020.128647.
82. Sri, S.; Chauhan, D.; Lakshmi, G.B.V.S.; Thakar, A.; Solanki, P.R. MoS2 nanoflower based electrochemical biosensor for TNF alpha detection in cancer patients. *Electrochimica Acta* **2022**, 405, 139736. https://doi.org/10.1016/j.electacta.2021.139736.
83. Hu, T.; Zhang, M.; Wang, Z.; Chen, K.; Li, X.; Ni, Z.H. Layer-by-layer self-assembly of MoS2/PDDA hybrid film in microfluidic chips for ultrasensitive electrochemical immunosensing of alpha-fetoprotein. *Microchemical Journal* **2020**, 158, 105209. https://doi.org/10.1016/j.microc.2020.105209.
84. Hu, D.; Cui, H.; Wang, X.; Luo, F.; Qiu, B.; Cai, W.; Huang, H.; Wang, J.; Lin, Z. Highly Sensitive and Selective Photoelectrochemical Aptasensors for Cancer Biomarkers Based on MoS2/Au/GaN Photoelectrodes. *Anal Chem.* **2021**, 93 (19), 7341-7347. doi: 10.1021/acs.analchem.1c01197.
85. Wei, Q.; Wang, C.; Li, P.; Wu, T.; Yang, N.; Wang, X.; Wang, Y.; Li, C. MOF Photochemistry: ZnS/C/MoS2 Nanocomposite Derived from Metal–Organic Framework for High-Performance Photo-Electrochemical Immunosensing of Carcinoembryonic Antigen. *Small* **2019**, 15, 1970257. https://doi.org/10.1002/smll.201970257.
86. Su, S.; Han, X.Y.; Lu, Z.W.; Liu, W.; Zhu, D.; Chao, J.; Fan, C.; Wang, L.H.; Song, S.P.; Lixing Weng, et al. Facile Synthesis of a MoS2-Prussian Blue Nanocube Nanohybrid-Based Electrochemical Sensing Platform for Hydrogen Peroxide and Carcinoembryonic Antigen Detection. *ACS Applied Materials & Interfaces* **2017**, 9 (14), 12773-12781. DOI: 10.1021/acsami.7b01141.
87. Wang, Y.g.; Zhao, G.h.; Zhang, Y.; Pang, X,h.; Cao, W.; Du, B.; Wei, Q. Sandwich-type electrochemical immunosensor for CEA detection based on Ag/MoS2@Fe3O4 and an analogous ELISA method with total internal reflection microscopy. *Sensors and Actuators B: Chemical* **2018**, 266, 561-569. https://doi.org/10.1016/j.snb.2018.03.178.
88. Liu, L.; Wei, Y,; Jiao, S.; Zhu, S.Y.; Liu, X.L. A novel label-free strategy for the ultrasensitive miRNA-182 detection based on MoS2/Ti3C2 nanohybrids. *Biosensors and Bioelectronics* **2019**, 137, 45-51. https://doi.org/10.1016/j.bios.2019.04.059.
89. Su, S.; Sun, Q.; Wan, L.; Gu, X.d.; Zhu, D.; Zhou, Y.; Chao, J.; Wang, L.H. Ultrasensitive analysis of carcinoembryonic antigen based on MoS2-based electrochemical immunosensor with triple signal amplification. *Biosensors and Bioelectronics* **2019**, 140, 111353. https://doi.org/10.1016/j.bios.2019.111353.
90. Lin, Y.; Xiong, C.; Shi, J.; Zhang,J.J.; Wang, X.H. Electrochemical immunosensor based on Pd@Pt/MoS2-Gr for the sensitive detection of CEA. *J Solid State Electrochem* **2021**, 25, 2075–2085. https://doi.org/10.1007/s10008-021-04978-y.
91. Li, S.; Hu, C.; Chen, C.; Zhang, J.w.; Bai, Y.C.; Tan, C.S.; Ni, G.J.; He, F.; Li, W.F.; Ming, D. Molybdenum Disulfide Supported on Metal-Organic Frameworks as an Ultrasensitive Layer for the Electrochemical

Detection of the Ovarian Cancer Biomarker CA125. *ACS Applied Bio Materials* **2021**, 4 (7), 5494-5502. DOI: 10.1021/acsabm.1c00324.

92. Mehmandoust, M.; Karimi, F.; Erk, N. A zinc oxide nanorods/molybdenum disulfide nanosheets hybrid as a sensitive and reusable electrochemical sensor for determination of anti-retroviral agent indinavir. *Chemosphere* **2022**, 300, 134430. https://doi.org/10.1016/j.chemosphere.2022.134430.
93. Li, W.J.; Qiao, X.W.; Hong, C.L.; Ma, C.Y.; Song, Y.J. A sandwich-type electrochemical immunosensor for detecting CEA based on CeO2-MoS2 absorbed Pb2+. *Analytical Biochemistry* **2020**, 592, 113566. https://doi.org/10.1016/j.ab.2019.113566.
94. Wang, Y.G.; Wang, Y.L.; Wu, D.; Ma, H.; Zhang, Y.; Fan, D.W.; Pang, X,H.; Du, B.; Wei, Q. Label-free electrochemical immunosensor based on flower-like Ag/MoS2/rGO nanocomposites for ultrasensitive detection of carcinoembryonic antigen. *Sensors and Actuators B: Chemical* **2018**, 255 (1), 125-132. https://doi.org/10.1016/j.snb.2017.07.129.
95. Gao, Z.Q.; Li Y.Y.; Zhang, X.B.; Feng, J.H.; Kong, L.; Wang, P.; Chen, Z.W.; Dong, Y.H.; Wei, Q. Ultrasensitive electrochemical immunosensor for quantitative detection of HBeAg using Au@Pd/MoS2@MWCNTs nanocomposite as enzyme-mimetic labels. *Biosensors and Bioelectronics* **2018**, 102, 189-195. https://doi.org/10.1016/j.bios.2017.11.032.
96. Pei, F.B.; Wang, P.; Ma, E.H.; Yang, Q.S.; Yu, H.X.; Liu, J.; Yin, H.H.; Li, Y.Y.; Liu, Q.; Dong, Y.H. A sensitive label-free immunosensor for alpha fetoprotein detection using platinum nanodendrites loaded on functional MoS2 hybridized polypyrrole nanotubes as signal amplifier. *Journal of Electroanalytical Chemistry* **2019**, 835, 197-204. https://doi.org/10.1016/j.jelechem.2019.01.037.
97. Soni, A.; Pandey, C.M.; Pandey, M.K.; Sumana, G. Highly efficient Polyaniline-MoS2 hybrid nanostructures based biosensor for cancer biomarker detection. *Analytica Chimica Acta* **2019**, 1055, 26-35. https://doi.org/10.1016/j.aca.2018.12.033.
98. Wang, C.; Wu, T.; Wang, X.; Wei, Q.; Wang, Y.Y.; Li, C.Y.; Sun, D. Ultrathin-layered carbon intercalated MoS2 hollow nanospheres integrated with gold nanoparticles for photoelectrochemical immunosensing of squamous cell carcinoma antigen. *Sensors and Actuators B: Chemical* **2019**, 297, 126716. https://doi.org/10.1016/j.snb.2019.126716.
99. Hou, S.N.; Wang, P.L.; Nie, Y.X.; Guo, Y.P.; Ma, Q. A novel work function tuning strategy-based ECL sensor with sulfur dots and Au NP@MoS2 nanosheet heterostructure for triple-negative breast cancer diagnosis. *Chemical Engineering Journal* **2022**, 446 (1), 136906. https://doi.org/10.1016/j.cej.2022.136906.
100. Singh, A.K.; Mittal, S.; Das, M.; Saharia, A.; Tiwari, M. Optical biosensors: a decade in review. *Alexandria Engineering Journal* **2023**, 67, 673-691. https://doi.org/10.1016/j.aej.2022.12.040.
101. Lv, Q.; Chen, L.S.; Liu, H.X.; Zou, L.L. Peony-like 3D-MoS2/graphene nanostructures with enhanced mimic peroxidase performance for colorimetric determination of dopamine. *Talanta* **2022**, 247, 123553. doi: 10.1016/j.talanta.2022.123553.
102. Guo, X.; Wang, Y.; Wu, F.; Ni, Y.; Kokot, S. A colorimetric method of analysis for trace amounts of hydrogen peroxide with the use of the nano-properties of molybdenum disulfide. *Analyst*. **2015**, 140 (4), 1119-26. doi: 10.1039/c4an01950d.
103. Zhao, L.; Wang, J.; Su, D.; Zhang, Y.; Lu, H.; Yan, X.; Bai, J.; Gao, Y.; Lu, G. The DNA controllable peroxidase mimetic activity of MoS2 nanosheets for constructing a robust colorimetric biosensor. *Nanoscale* **2020**, 12 (37), 19420-19428. doi: 10.1039/d0nr05649a.
104. Su S, Li J, Yao Y, Sun, Q.; Zhao, Q.; Wang. F.; Li. Q.; Liu, X.; Wang, L. Colorimetric Analysis of Carcinoembryonic Antigen Using Highly Catalytic Gold Nanoparticles. *ACS Applied bio Materials* **2019**, 2 (1), 292-298. DOI: 10.1021/acsabm.8b00598. 87.
105. Wang, X.; Cheng, S.; Wang, X.; Wei, L.; Kong, Q.; Ye, M.; Luo, X.; Xu, J.; Zhang, C.; Xian, Y. pH-Sensitive Dye-Based Nanobioplatform for Colorimetric Detection of Heterogeneous Circulating Tumor Cells. *ACS Sens* **2021**, 6 (5), 1925-1932. doi: 10.1021/acssensors.1c00314.
106. Ma, C.; Cao, Y.; Gou, X.; Zhu, J.J. Recent Progress in Electrochemiluminescence Sensing and Imaging. *Anal Chem.* **2020**, 92 (1), 431-454. doi: 10.1021/acs.analchem.9b04947.
107. Zhang, S.; Liu, Y. Recent Progress of Novel Electrochemiluminescence Nanoprobes and Their Analytical Applications. *Front Chem.* **2021**, 8, 626243. doi: 10.3389/fchem.2020.626243.
108. Lv, X.; Li, Y.; Cui, B.; Fang, Y.; Wang, L. Electrochemiluminescent sensor based on an aggregation-induced emission probe for bioanalytical detection. *Analyst.* **2022**, 147 (11), 2338-2354. doi: 10.1039/d2an00349j.

109. Du, L.; Zhang, H.; Wang, Z.; Zhuang, T.; Wang, Z. Boosting the electrochemiluminescence of luminol by high-intensity focused ultrasound pretreatment combined with 1T/2H MoS2 catalysis to construct a sensitive sensing platform. *Ultrason Sonochem*. **2023**, 92, 106264. doi: 10.1016/j.ultsonch.2022.106264.
110. Ma, C.; Zhang, Z.; Tan, T.; Zhu, J.J. Recent Progress in Plasmonic based Electrochemiluminescence Biosensors: A Review. *Biosensors (Basel)* **2023**, 13 (2), 200. doi: 10.3390/bios13020200.
111. Zhang, Z.; Yu, H.; Zhang, Y.; Wang, Z.; Gao, H.; Rong, S.; Meng, L.; Dai, J.; Pan, H.; Chang, D. A sandwich-configuration electrochemiluminescence immunoassay based on Cu2O@OMC-Ru nanocrystals and OMC-MoS2 nanocomposites for determination of alpha-fetoprotein. *Mikrochim Acta.* **2021**, 188 (6), 213. doi: 10.1007/s00604-021-04848-4.
112. Srinidhi, G.; Sudalaimani, S.; Giribabu, K.; Basha, S.J.S.; Suresh, C. Amperometric determination of hydrazine using a CuS-ordered mesoporous carbon electrode. *Mikrochim Acta.* **2020**, 187 (6), 359. doi: 10.1007/s00604-020-04325-4.
113. Liu, Y.; Nie, Y.; Wang, M.; Zhang, Q.; Ma, Q. Distance-dependent plasmon-enhanced electrochemiluminescence biosensor based on MoS2 nanosheets. *Biosens Bioelectron.* **2020**, 148, 111823. doi: 10.1016/j.bios.2019.111823.
114. Muhammad, M.; Khan, S.; Shehzadi, S.A.; Gul, Z.; Al-Saidi, H.M.; Kamran, A.W.; Alhumaydhi, F.A. Recent advances in colorimetric and fluorescent chemosensors based on thiourea derivatives for metallic cations: A review. *Dyes and Pigments* **2022**, 205, 110477. https://doi.org/10.1016/j.dyepig.2022.110477.
115. Yao W, Ling J, Zhang W, Ding Y. Highly sensitive fluorescent aptasensor based on MoS2 nanosheets for one-step determination of methamphetamine. *Anal Sci.* **2022**, 38 (1), 99-104. doi: 10.2116/analsci.21P144.
116. Liang, J.; Yan, R.; Chen, C.; Yao, X.; Guo, F.; Wu, R.; Zhou, Z.; Chen, J.; Li G. A novel fluorescent strategy for Golgi protein 73 determination based on aptamer/nitrogen-doped graphene quantum dots/molybdenum disulfide @ reduced graphene oxide nanosheets. *Spectrochim Acta A Mol Biomol Spectrosc* 2023, 294, 122538. doi: 10.1016/j.saa.2023.122538.
117. Wang, J.J.; Liu, Y.; Ding, Z.; Zhang, L.; Han, C.; Yan, C.; Amador, E.; Yuan, L.; Wu, Y.; Song, C.; et al. The exploration of quantum dot-molecular beacon based MoS2 fluorescence probing for myeloma-related Mirnas detection. *Bioact Mater.* **2022**, 17, 360-368. doi: 10.1016/j.bioactmat.2021.12.036.
118. Chhowalla, M.; Shin, H.S.; Eda, G.; Li, L.J.; Loh, K.P.; Zhang, H. The chemistry of two-dimensional layered transition metal dichalcogenide nanosheets. *Nat Chem.* **2013**, 5 (4), 263-75. doi: 10.1038/nchem.1589.
119. Ge, J.; Hu, Y.;, Deng, R., Li, Z.; Zhang, K.; Shi, M.; Yang, D.; Cai, R.; Tan, W. Highly Sensitive MicroRNA Detection by Coupling Nicking-Enhanced Rolling Circle Amplification with MoS2 Quantum Dots. *Anal Chem.* **2020**, 92 (19), 13588-13594. doi: 10.1021/acs.analchem.0c03405.
120. Strobbia, P.; Cupil-Garcia, V.; Crawford, B.M.; Fales, A.M.; Pfefer, T.J.; Liu, Y.; Maiwald, M.; Sumpf, B.; Vo-Dinh, T. Accurate in vivo tumor detection using plasmonic-enhanced shifted-excitation Raman difference spectroscopy (SERDS). *Theranostics* **2021**, 11 (9), 4090-4102. doi: 10.7150/thno.53101.
121. Er, E.; Sánchez-Iglesias, A.; Silvestri, A.; Arnaiz, B.; Liz-Marzán, L.M.; Prato, M.; Criado, A. Metal Nanoparticles/MoS2 Surface-Enhanced Raman Scattering-Based Sandwich Immunoassay for $\alpha$-Fetoprotein Detection. *ACS Appl Mater Interfaces* **2021**, 13 (7), 8823-8831. doi: 10.1021/acsami.0c22203.
122. Pan, H.; Dong, Y.; Gong, L.; Zhai, J.; Song, C.; Ge, Z.; Su, Y.; Zhu, D.; Chao, J.; Su, S.; et al. Sensing gastric cancer exosomes with MoS2-based SERS aptasensor. *Biosens Bioelectron* **2022**, 215, 114553. doi: 10.1016/j.bios.2022.114553.
123. Medetalibeyoglu, H.; Kotan, G.; Atar, N.; Yola, M.L. A novel sandwich-type SERS immunosensor for selective and sensitive carcinoembryonic antigen (CEA) detection. *Anal Chim Acta.* **2020**, 1139, 100-110. doi: 10.1016/j.aca.2020.09.034.
124. Samy, O.; Zeng, S.; Birowosuto, M.D.; El Moutaouakil, A. A Review on MoS2 Properties, Synthesis, Sensing Applications and Challenges. *Crystals* **2021**, 11, 355. https://doi.org/10.3390/cryst11040355.
125. Chiu, N.F.; Yang, H.T. High-Sensitivity Detection of the Lung Cancer Biomarker CYFRA21-1 in Serum Samples Using a Carboxyl-MoS2 Functional Film for SPR-Based Immunosensors. *Front Bioeng Biotechnol* **2020**, 8, 234. doi: 10.3389/fbioe.2020.00234.
126. Xin, W.L.; Jiang, L.F.; Zong, L.P.; Zeng, H.B.; Shu, G.F.; Marks, R.; Zhang, X.J.; Shan, D. MoS2 quantum dots-combined zirconium-metalloporphyrin frameworks: Synergistic effect on electron transfer and application for bioassay. *Sensors and Actuators B: Chemical* **2018**, 273, 566-573. https://doi.org/10.1016/j.snb.2018.06.090.

127. Hou, F.; Hu, X.B.; Ma, S.H.; Cao, J.T.; Liu, Y.M. Construction of electrochemiluminescence sensing platform with in situ generated coreactant strategy for sensitive detection of prostate specific antigen. *Journal of Electroanalytical Chemistry* **2020**, 858, 113817. https://doi.org/10.1016/j.jelechem.2019.113817.
128. Nie, Y.X.; Zhang, X.; Zhang, Q.; Liang, Z.H.; Ma, Q.; Su, X.G. A novel high efficient electrochemiluminescence sensor based on reductive Cu(I) particles catalyzed Zn-doped MoS2 QDs for HPV 16 DNA determination. *Biosensors and Bioelectronics* **2020**, 160, 112217. https://doi.org/10.1016/j.bios.2020.112217.
129. Hou, S.N.; Wang, P.L.; Nie, Y.X.; Guo, Y.P.; Ma, Q. A novel work function tuning strategy-based ECL sensor with sulfur dots and Au NP@MoS2 nanosheet heterostructure for triple-negative breast cancer diagnosis. *Chemical Engineering Journal* **2022**, 446 (1), 136906. https://doi.org/10.1016/j.cej.2022.136906.
130. Liu, W.; Su, M.L.; Chen, A.; Peng, K.F.; Chai, Y.Q.; Yuan, R. Highly Efficient Electrochemiluminescence Based on Luminol/MoS2 Quantum Dots@Zeolitic Imidazolate Framework-8 as an Emitter for Ultrasensitive Detection of MicroRNA. *Analytical Chemistry* **2022**, 94, (25), 9106-9113.DOI: 10.1021/acs.analchem.2c01444.
131. Lianjing Zhao, Dehao Kong, Zepei Wu, Guannan Liu, Yuan Gao, Xu Yan, Fangmeng Liu, Xiaomin Liu, Chenguang Wang, Jiuwei Cui, et al. Interface interaction of MoS2 nanosheets with DNA based aptameric biosensor for carbohydrate antigen 15–3 detection. *Microchemical Journal* **2020**, 155, 104675. https://doi.org/10.1016/j.microc.2020.104675.
132. Peng, X.; Wang, Y.; Wen, W.; Chen, M.M.; Zhang, X.; Wang, S. Simple MoS2-Nanofiber Paper-Based Fluorescence Immunosensor for Point-of-Care Detection of Programmed Cell Death Protein 1. *Anal Chem.* **2021**, 93 (25), 8791-8798. doi: 10.1021/acs.analchem.1c00269.
133. Jiang, J.; Liu, H.; Li, X.; Chen, Y.; Gu, C.; Wei, G.; Zhou, J.; Jiang, T. Nonmetallic SERS-based immunosensor byintegrating MoS2 nanoflower and nanosheet towards the direct serum detection of carbohydrate antigen 19-9. *Biosens Bioelectron*. **2021**, 193, 113481. doi: 10.1016/j.bios.2021.113481.
134. van der Zande, A.M.; Huang, P.s.Y.; Chenet, D.A.; Berkelbach, T.C.; You, Y.M.; Lee, G.H.; Heinz, T.F.; Reichman, D.R.; Muller D.A.; Hone, J.C. Grains and grain boundaries in highly crystalline monolayer molybdenum disulphide. *Nature Mater* **2013**, 12, 554-561. https://doi.org/10.1038/nmat3633.
135. Shi, J.Y; Qin, W.L.; Lin, Y.; Li, M.X.; Wu, Y.Y.; Luo, H.; Yan, J.; Huang, K.J.; Tan, X.X. Enhancing biosensing with fourfold amplification and self-powering capabilities: MoS2@C hollow nanorods-mediated DNA hexahedral framework architecture for amol-level liver cancer tumor marker detection. *Analytica Chimica Acta* **2023**, 1271, 341413. https://doi.org/10.1016/j.aca.2023.341413.
136. Wang, R.; Liu, H.; Xu, T.; Zhang, Y.; Gu, C.; Jiang, T. SERS-based recyclable immunoassay mediated by 1T-2H mixed-phase magnetic molybdenum disulfide probe and 2D graphitic carbon nitride substrate. *Biosens Bioelectron*. **2023**, 227, 115160. doi: 10.1016/j.bios.2023.115160.
137. Yang, Y.; Zeng, B.; Li, Y.; Liang, H.G.; Yang Y.B.; Yuan,Q. Construction of MoS2 field effect transistor sensor array for the detection of bladder cancer biomarkers. *Sci. China Chem.* **2020**, 63, 997-1003. https://doi.org/10.1007/s11426-020-9743-2.
138. Zhang, Y.; Feng, D.Z.; Xu, Y.; Yin, Z.W.; Dou, W.; Habiba, U.M.E.; Pan, C.Y.; Zhang, Z.k.; Mou, H.; Deng, H.y.; et al. DNA-based functionalization of two-dimensional MoS2 FET biosensor for ultrasensitive detection of PSA. *Applied Surface Science* **2021**, 548, 149169. https://doi.org/10.1016/j.apsusc.2021.149169.
139. Kashefi-Kheyrabadi, L.; Kim, J.; Chakravarty, S.; Park, S.y.; Gwak, H.; Kim, S.; Mohammadniaei, M. Lee, M.H.; Hyun, K.A.; Jung, H. Detachable microfluidic device implemented with electrochemical aptasensor (DeMEA) for sequential analysis of cancerous exosomes. *Biosensors and Bioelectronics* **2020**, 169, 112622. https://doi.org/10.1016/j.bios.2020.112622.
140. Yagati, A.K.; Go, A.; Vu, N.H.; Lee, M.H. A MoS2–Au nanoparticle-modified immunosensor for T3 biomarker detection in clinical serum samples. *Electrochimica Acta* **2020**, 342, 136065. https://doi.org/10.1016/j.electacta.2020.136065.
141. Jandas, P.J.; Luo, J.T.; Prabakaran, K.; Chen, F.; Fu, Y.Q. Highly stable, love-mode surface acoustic wave biosensor using Au nanoparticle-MoS2-rGO nano-cluster doped polyimide nanocomposite for the selective detection of carcinoembryonic antigen. *Materials Chemistry and Physics* **2020**, 246, 122800. https://doi.org/10.1016/j.matchemphys.2020.122800.
142. Torul, H.; Yarali, E.; Eksin, E.; Ganguly, A.; Benson, J.; Tamer, U.; Papakonstantinou, P.; Erdem, A. Paper-Based Electrochemical Biosensors for Voltammetric Detection of miRNA Biomarkers Using Reduced

Graphene Oxide or MoS2 Nanosheets Decorated with Gold Nanoparticle Electrodes. *Biosensors* **2021**, 11, 236. https://doi.org/10.3390/bios11070236

143. Zhou, C.X.; Cui, K.; Liu, Y.; Li, L.; Zhang, L.; Hao, S.J.; Ge, S,G.; Yu, J,H. Bi2S3@MoS2 Nanoflowers on Cellulose Fibers Combined with Octahedral CeO2 for Dual-Mode Microfluidic Paper-Based MiRNA-141 Sensors. *ACS Applied Materials & Interfaces* **2021**, 13 (28), 32780-32789. DOI: 10.1021/acsami.1c07669
144. Ma, J.L.; Xue, D.; Xu, T.; Wei, G.D.; Gu, C.J.; Zhang, Y.L.; Jiang, T. Nonmetallic SERS-based biosensor for ultrasensitive and reproducible immunoassay of ferritin mediated by magnetic molybdenum disulfide nanoflowers and black phosphorus nanosheets. *Colloids and Surfaces B: Biointerfaces* **2023**, 227, 113338. https://doi.org/10.1016/j.colsurfb.2023.113338.
145. Rahman, M.T.; Kumar, R.; Kumar, M.; Qiao, Q.Q. Two-dimensional transition metal dichalcogenides and their composites for lab-based sensing applications: Recent progress and future outlook. *Sensors and Actuators A: Physical* **2021**, 318, 112517. https://doi.org/10.1016/j.sna.2020.112517.
146. Nakada, G.; Igarashi, Y.; Imai, H.; Oaki, Y. Materials-Informatics-Assisted High-Yield Synthesis of 2D Nanomaterials through Exfoliation. *Adv. Theory Simul.* **2019**, 2, 1800180. https://doi.org/10.1002/adts.201800180.
147. Sethulekshmi, A.S.; Saritha, A.; Joseph, K.; Aprem, A.S.; Sisupal, S.B. MoS2 based nanomaterials: Advanced antibacterial agents for future. *Journal of Controlled Release* **2022**, 348, 158-185.https://doi.org/10.1016/j.jconrel.2022.05.047.
148. Manzeli, S.; Dumcenco, D.; Migliato Marega, G.; Kis, A. Self-sensing, tunable monolayer MoS2 nanoelectromechanical resonators. *Nat Commun.* **2019**, 10 (1), 4831. doi: 10.1038/s41467-019-12795-1.
149. Siao, M.D.; Shen, W.C.; Chen, R.S.; Chang, Z.W.; Shih, M.C.; Chiu, Y.P.; Cheng, C.M. Two-dimensional electronic transport and surface electron accumulation in MoS2. *Nat Commun* **2018**, 9, 1442. https://doi.org/10.1038/s41467-018-03824-6.
150. Tsai, Y.C.; Li, Y. Impact of Doping Concentration on Electronic Properties of Transition Metal-Doped Monolayer Molybdenum Disulfide. *IEEE Transactions on Electron Devices* **2018**, 65, 2, 733-738. doi: 10.1109/TED.2017.2782667.
151. Hu, T.; Zhang, R.; Li, J.P.; Cao, J.Y.; Qiu, F. Photodetectors based on two-dimensional MoS2 and its assembled heterostructures. *Chip* **2022**, 1 (3), 100017. https://doi.org/10.1016/j.chip.2022.100017.
152. Kaur, J.; Singh, M.; Dell'Aversana, C.; Benedetti, R.; Giardina, P.; Rossi, M.; Valadan, M.; Vergara, A.; Cutarelli, A.; Montone, A.M.I.; et al. Biological interactions of biocompatible and water-dispersed MoS2 nanosheets with bacteria and human cells. *Sci Rep.* **2018**, 68 (1), 16386. doi: 10.1038/s41598-018-34679-y.
153. Mohan, M.; Shetti, N.P.; Aminabhavi, T.M. Recent developments in MoS2-based flexible supercapacitors. Materials *Today Chemistry* **2023**, 27, 101333. https://doi.org/10.1016/j.mtchem.2022.101333.